



## Multi-centennial summer and winter precipitation variability in southern South America

R. Neukom,<sup>1,2</sup> J. Luterbacher,<sup>3</sup> R. Villalba,<sup>4</sup> M. Küttel,<sup>1,2,5</sup> D. Frank,<sup>2,6</sup> P. D. Jones,<sup>7</sup> M. Grosjean,<sup>1,2</sup> J. Esper,<sup>8</sup> L. Lopez,<sup>4</sup> and H. Wanner<sup>1,2</sup>

Received 20 April 2010; revised 9 June 2010; accepted 16 June 2010; published 31 July 2010.

[1] We present the first spatially and temporally highly resolved gridded reconstruction of multi-centennial precipitation variability for southern South America (SSA). A novel reconstruction approach of deriving 10,000 ensemble members based on varying predictor networks and methodological settings allows the identification of spatiotemporal changes in SSA precipitation and associated uncertainties. The summer and winter reconstructions back to AD 1498 and AD 1590, respectively, provide new evidence for multi-centennial increase in summer precipitation and an opposing decrease in winter precipitation into the 20th century. The drying in winter is significant over large parts of SSA, whereas the patterns for summer, possibly representing convective rainfall, have displayed high spatial variability. The fact that such long-term seasonal and spatial changes have occurred in the past, underlines the complex form that hydroclimatic variability might have in the future. This emphasizes the need for careful adaptation strategies as governments become attuned to the realities of climate change. **Citation:** Neukom, R., J. Luterbacher, R. Villalba, M. Küttel, D. Frank, P. D. Jones, M. Grosjean, J. Esper, L. Lopez, and H. Wanner (2010), Multi-centennial summer and winter precipitation variability in southern South America, *Geophys. Res. Lett.*, 37, L14708, doi:10.1029/2010GL043680.

### 1. Introduction

[2] The fundamental dependence of all living beings on water makes projected spatial, temporal, and seasonal variations in water-supply a critical factor in determining how well societies can adapt to on-going climate change. Furthermore, changes in the seasonal patterns and cycles may also have significant consequences on snow versus rain totals, runoff rates and ecosystem functioning and accord-

ingly require new agricultural practices. Knowledge of past variations in the hydrological cycle is of crucial importance for placing recent moisture changes on local, regional and continental scales into a long term context and understanding the processes driving these changes [Jansen *et al.*, 2007; Jones *et al.*, 2009]. However, gridded (proxy based) reconstructions of moisture variability are still rare and predominantly restricted to the Northern Hemisphere [e.g., Cook *et al.*, 2004, 2010; Pauling *et al.*, 2006], mostly due to the limited number of annually-resolved precipitation-sensitive proxy data available.

[3] Due to the modulating effect of the Andes and the influence of distinct oceanic and atmospheric patterns such as the El Niño–Southern Oscillation, the Southern Annular Mode, and the South American Summer Monsoon, South America’s precipitation regime is particularly variable [e.g., Garreaud *et al.*, 2009] (see also Figure 1). Considering that South America’s economies and societies are highly dependent on hydropower generation and irrigation [Magrin *et al.*, 2007], it is important to quantify past and present precipitation variability and extremes in this region as detailed as possible.

[4] In southern South America (SSA, south of 20°S), the number of precipitation-sensitive records from paleoclimatic archives, such as tree rings [Boninsegna *et al.*, 2009], documentary evidence [e.g., Neukom *et al.*, 2009] and lake sediments [e.g., Moy *et al.*, 2009] has significantly increased within the last decade. Herein, we combine the currently available annually or higher resolved paleoclimatic evidence with long instrumental data to derive gridded (0.5° × 0.5°), seasonal SSA precipitation reconstructions. Separately reconstructed austral summer and winter precipitation fields with associated uncertainties are provided back to the late 15th (summer) and 16th (winter) centuries. These reconstructions represent the first spatially explicit estimates of large-scale SSA precipitation prior to the instrumental era.

### 2. Data and Methods

#### 2.1. Instrumental Calibration Data

[5] We use the new 0.5° × 0.5° and monthly resolved CRU TS 3 gridded precipitation dataset (updated from Mitchell and Jones [2005]) covering 1901–2006 as instrumental target. The SSA region is defined as all land grid cells between 20°S–55°S and 80°W–30°W. The reconstructions are performed for austral summer (December to February; DJF) and winter (June to August; JJA). These seasons were selected based upon tests of the optimal seasonal response windows of the proxy records (not shown). We used the period 1931–1995 for generating ensemble calibration/verification reconstructions. Before 1931, the

<sup>1</sup>Institute of Geography, Climatology and Meteorology, University of Bern, Bern, Switzerland.

<sup>2</sup>Oeschger Centre for Climate Change Research, University of Bern, Bern, Switzerland.

<sup>3</sup>Department of Geography, Climatology, Climate Dynamics and Climate Change, Justus Liebig University Giessen, Giessen, Germany.

<sup>4</sup>Instituto Argentino de Nivología y Glaciología y Ciencias Ambientales, CONICET, Mendoza, Argentina.

<sup>5</sup>Department of Earth and Space Sciences, University of Washington, Seattle, Washington, USA.

<sup>6</sup>Swiss Federal Research Institute WSL, Birmensdorf, Switzerland.

<sup>7</sup>Climatic Research Unit, School of Environmental Sciences, University of East Anglia, Norwich, UK.

<sup>8</sup>Department of Geography, Johannes Gutenberg University, Mainz, Germany.

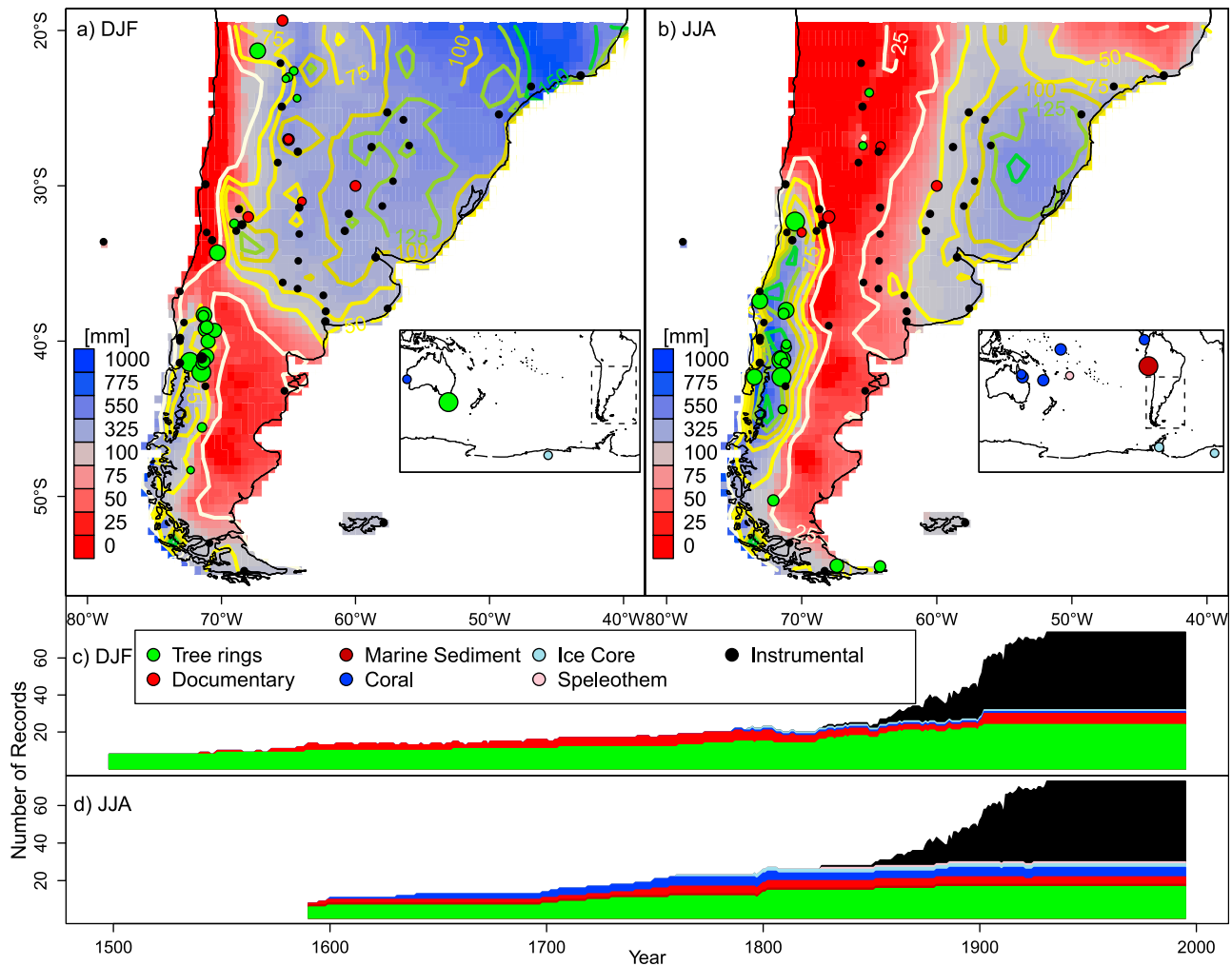


**Figure 1.** Locations of the predictors used for the (a) summer and (b) winter reconstructions. The size of the circles represents the lengths of the series (smallest: 90 years, largest: >1000 years). The reconstruction area is marked by a dashed margin in the small maps. Shaded colors in the SSA-maps represent the 1931–1995 average precipitation [mm]. Notice the different scale in the reddish and bluish colors. The contour lines indicate precipitation standard deviations 1931–1995 [mm]. Temporal evolution of the number of predictors used for (c) summer and (d) winter.

quality of the gridded data is reduced due to a strong decline in available station data [see, e.g., Garreaud *et al.*, 2009; Neukom *et al.*, 2010].

## 2.2. Predictor Data

[6] As a basis for the selection of the predictors, we use the SSA proxy network established by Neukom *et al.* [2010] consisting of 144 natural proxies (tree rings, ice cores, corals, speleothems, lake and marine sediments) and documentary records sensitive to SSA climate. From this network, the records significantly correlating with the instrumental target in the overlapping period are selected (see auxiliary material).<sup>1</sup> Additionally, long instrumental precipitation series from SSA (GHCN [Peterson and Vose, 1997]) with data prior to 1920 and covering at least 50 years within the 1931–1995 calibration window are included as predictors. Table S1 (Table S2) presents the final predictor network consisting of 33 (31) proxy records and 41 (42) instrumental

series for summer (winter). The locations of the proxies as well as their temporal availability are shown in Figure 1. Some of the proxy records are related to SSA precipitation by large-scale teleconnection patterns [e.g., Villalba *et al.*, 1997]. Neukom *et al.* [2010] showed that consideration of such remote proxies can substantially improve SSA climate reconstructions. The selected predictors are fully independent from those used by Neukom *et al.* [2010] to reconstruct seasonal temperature fields. Missing values (<0.1%) in the predictor matrices during the calibration period were estimated using an EOF (empirical orthogonal functions) based algorithm [Neukom *et al.*, 2010; Scherrer and Appenzeller, 2006].

## 2.3. Reconstruction Methodology

[7] We performed the reconstructions using ordinary least squares principal component regression (PCR) [e.g., Küttel *et al.*, 2010; Luterbacher *et al.*, 2002, 2004; Neukom *et al.*, 2010; Pauling *et al.*, 2006; Xoplaki *et al.*, 2005]. In PCR, transfer functions between a certain number of principal components of the predictor and instrumental data

<sup>1</sup>Auxiliary materials are available in the HTML. doi:10.1029/2010GL043680.

are established in the calibration period using multiple linear regressions. This relationship is then used to predict the values of the predictand in the reconstruction period based on the assumption that the relationship is linear and stable over time (see *Luterbacher et al.* [2002] for a detailed discussion of the methodology). As the number of available predictors changes over time (Figures 1c and 1d and Tables S1 and S2), individual regression models are calculated using at each time step the maximum number of available predictors, resulting in a total of 88 (86) statistical models for winter (summer). To avoid variance biases due to the decreasing number of predictors back in time [e.g., *Cook et al.*, 2004; *Frank et al.*, 2007], the reconstructions of each model were scaled to the variance of the instrumental target in the 1931–1995 overlap period. It is well known that the selection of the predictors, calibration and verification periods, as well as parameters within the reconstruction methodology influence reconstructed values [e.g., *Rutherford et al.*, 2005; *Wahl and Ammann*, 2007]. Yet, as objective selection criteria are largely missing, we derive an ensemble of 10,000 reconstructions, with each member being based on different reconstruction settings [see also *Frank et al.*, 2010; *van der Schrier et al.*, 2007]. The settings are varied for each ensemble member by randomly (1) withholding five predictors from the predictor dataset; (2) choosing 43 (non-successive) years (corresponds to two thirds of all years) within the 1931–1995 overlap period for calibration. The remaining third (22 years) are used for verification; (3) varying the percentage of total variance explained by the retained PCs between 60% and 95%, corresponding to 8 (1) to 39 (13) PCs of the instrumental (predictor) data matrix. This is done individually for the instrumental as well as predictor matrices.

[8] Even with these settings, not all parameters in the reconstruction methodology are objectively considered. For example, withholding five predictors is a compromise between allowing reconstructions to be derived reasonably far back in time and introducing sufficient variability between ensemble members. Further, the range of PCs chosen to be retained is somewhat arbitrary, however representing the range commonly used in comparable reconstructions. Consequently, we obtain a distribution function for the reconstructed values, rather than a single value as for conventional methodologies. For the reconstruction of precipitation  $P$  at each location and time step, median values of the ensemble members (see Figure S1) are calculated. In order to minimize variance biases due to changes in the correlations between the 10,000 realizations,  $P$  is variance adjusted using the RUNNINGr-adjustment described by *Frank et al.* [2007]. It must be noted that uncertainties that may arise from systematic methodological biases, such as variance losses and mean biases [e.g., *Smerdon et al.*, 2010, and references therein], are not captured by our ensemble approach. Pre-

dictor data availability allows the reconstruction of SSA summer (winter) precipitation back to AD 1498 (1590), where eight predictors are available. Other reconstruction techniques were also tested (composite plus scaling and regularized expectation maximization). They yielded similar ensemble means, but lower regression skills and occasionally extreme outliers of single ensemble members [see also *Neukom et al.*, 2010; *Wilson et al.*, 2010]. We therefore confine our analysis to the results of PCR.

### 3. Results and Discussion

[9] The reconstructed spatial precipitation patterns, displayed as century-averaged anomalies relative to the 1931–1995 mean, indicate that austral summers of the 17th to 19th centuries were in most regions drier than climatology, particularly in the La Plata Basin and Patagonia (Figure 2). Anomalously wet conditions prevailed during this period in the subtropical Andes, north-eastern SSA and Tierra del Fuego. The 16th century shows a different picture with mostly positive (negative) anomalies north (south) of approximately 37° S. Except for some regions in northern Patagonia, Tierra del Fuego and north-eastern SSA, 17th to 19th century austral winters were generally wetter than climatology. The maps in the bottom row of Figure 2 depict the areas where the 1931–1995 period was drier (red) or wetter (blue) than all preceding centuries. Dark shadings delineate areas where all of the four (three) previous centuries were significantly ( $p < 0.05$ ; Wilcoxon test) drier or wetter than the 1931–1995 summers (winters). Modern summer conditions (1931–1995) are reconstructed to be significantly wetter than any of the preceding centuries' mean over entire Patagonia. Parts of north-western Argentina and north-eastern SSA are in contrast found to be drier. In winter, significant drying can be found across large areas of SSA. The only region where the change is significant and of the same sign in both seasons (dry 1931–1995) is north-western Argentina. Although we have shown how precipitation varies in space throughout time, it is also interesting to assess the temporal changes averaged over particular regions and the entire SSA domain. This is shown in Figure 3 (for alternative illustrations of the ensemble members see Figures S2–S5, statistical skill measures see section S3 and Figures S6–S12 of Text S1). Averaged over SSA, reconstructed summers are generally drier than climatology between 1600–1930 but slightly wetter in the 16th century. Winter conditions in the 17th to 19th centuries reveal an opposite picture with reconstructed precipitation mostly being above climatology. The robustness of these conclusions clearly changes over time, with the spread of the ensemble members decreasing towards the end of the 19th century when instrumental predictors become increasingly available. As an independent validation, Figure 3c shows our recon-

**Figure 2.** Average precipitation anomalies of the 16th (top row, only for summer), 17th (second row), 18th (third row) and 19th (fourth row) centuries relative to the calibration period (1931–1995). Contour lines indicate the average inter-annual reconstruction uncertainties in the respective century, defined as the root mean squared difference between the ensemble median  $P$  and the 5th and 95th percentiles of the ensembles, respectively. All values are shown relative to the instrumental standard deviation 1931–1995 in order to take account of the large regional variations in precipitation within SSA (Figure 1). Fifth row: Areas where all of the four (three) previous centuries were drier or wetter than the 1931–1995 summers (winters). Dark colors indicate significant results ( $p < 0.05$ ; Wilcoxon test). Left: summer; right: winter.

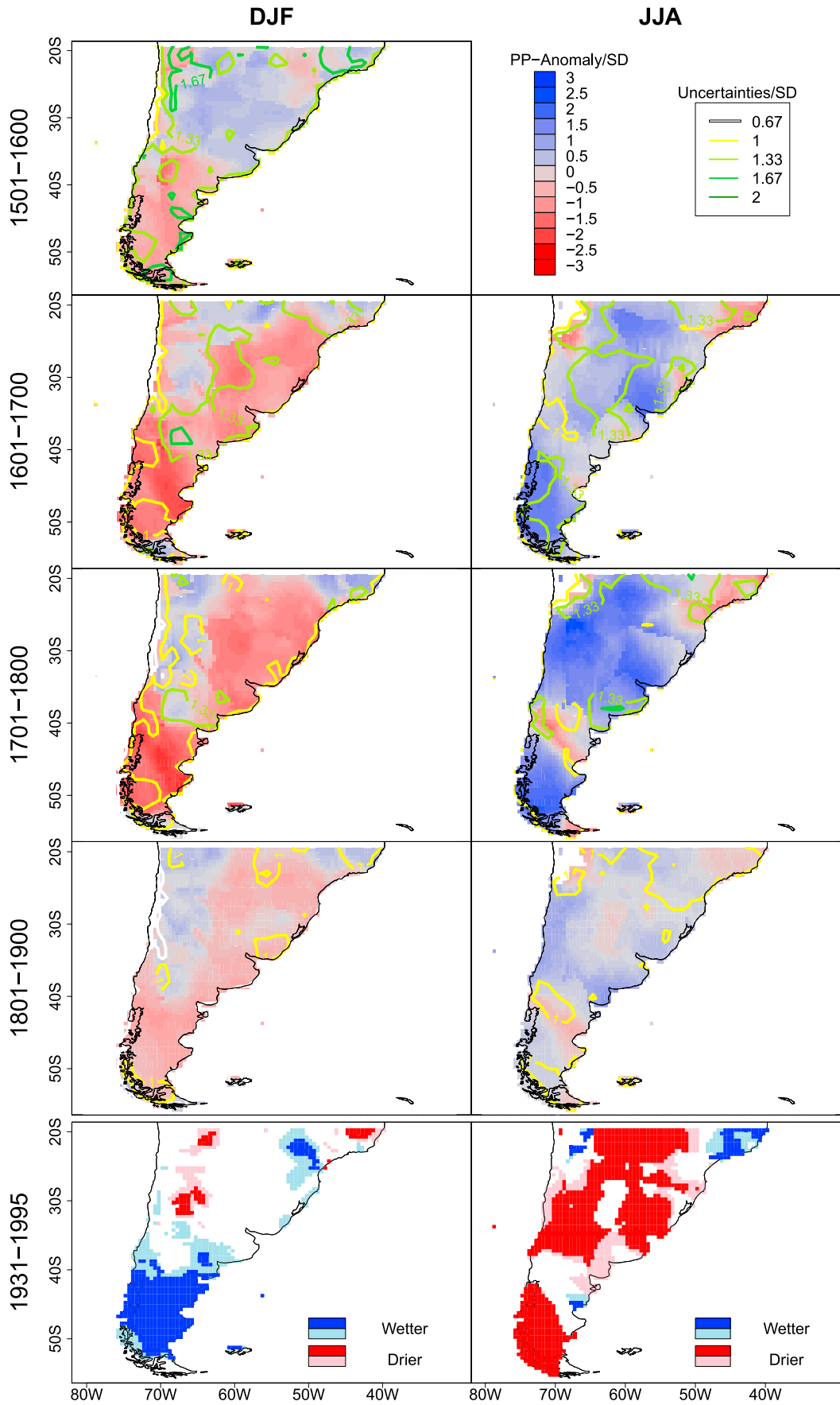
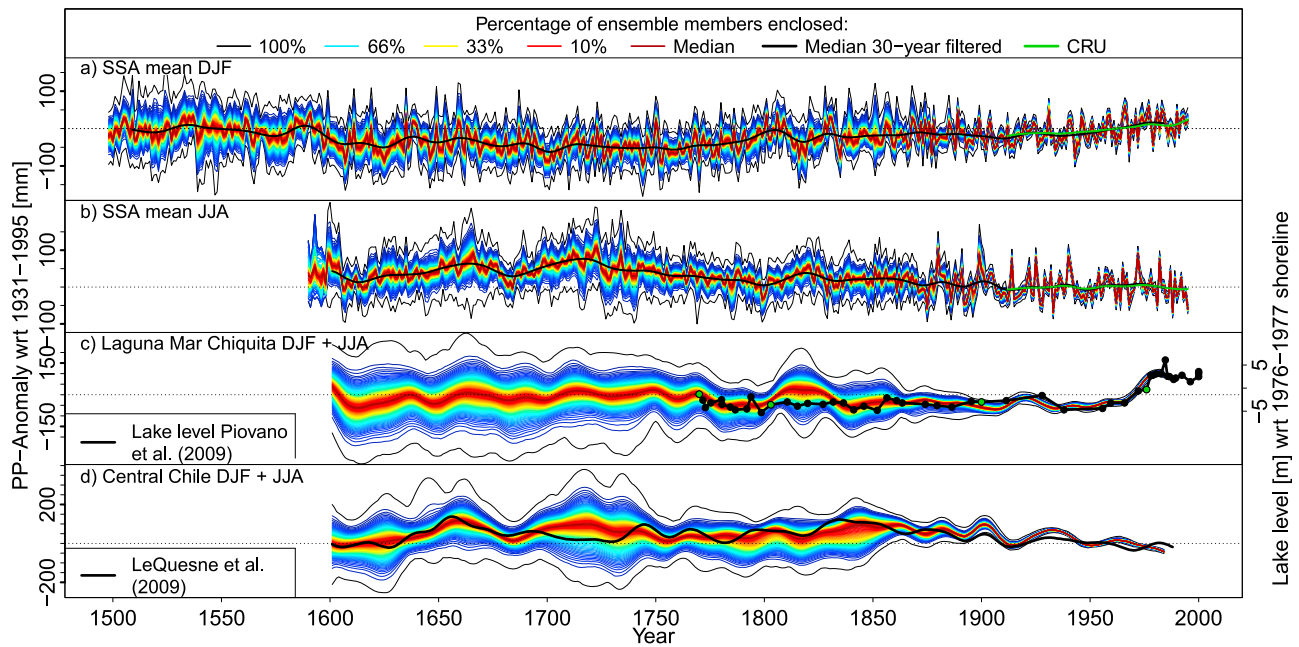


Figure 2



**Figure 3.** Percentiles of the reconstruction ensembles. Each line represents a percentile. The area between the black lines encloses all (100%) members; the area between the lowest (1st percentile) and the highest blue lines (99th percentile) encloses 98% of the members, and so on. SSA mean summer (winter) precipitation reconstruction (a) 1498–1995 and (b) 1590–1995, anomalously to the 1931–1995 average. Bold lines: 30-year Gaussian filtered ensemble median (black) and CRU gridded (green) precipitation. (c) 30-year Gaussian filtered annual precipitation (sum of summer and winter accounting for 63% of the annual instrumental precipitation totals) in the catchment area of Laguna Mar Chiquita and the lake level reconstruction of *Piovano et al.* [2009] (black, green points are dated, other dates are linearly interpolated). (d) 30-year filtered Central Chile annual precipitation (sum of summer and winter accounting for 78% of annual instrumental totals) compared to the results of *Le Quesne et al.* [2009] (black, 30-year filter).

struction (sum of summer and winter) averaged over the catchment area of the Laguna Mar Chiquita in northern Argentina along with the lake level reconstruction by *Piovano et al.* [2009] (for methodological details see the auxiliary material). Both curves indicate dry conditions between 1770 and 1950, followed by a sharp increase towards present. The pluvial period in the first half of the 19th century in our reconstruction is, however, not confirmed by the lake level reconstruction. In this period, the spread of our ensemble members is relatively large, indicating reduced reliability of the median values. Figure 3d presents our reconstruction (sum of summer and winter) in Central Chile along with the tree-ring based annual precipitation reconstruction of *Le Quesne et al.* [2009]. Again, the two reconstructions show similar decadal-scale fluctuations and the period with the largest discrepancy (early 18th century) corresponds to an episode of reduced agreement among ensemble members. Both validations reveal a good agreement over the data rich 20th century, indicating increasing (decreasing) precipitation amounts in the Laguna Mar Chiquita (Central Chile). Further back in time, reconstruction uncertainties (i.e. the spread of the ensemble members) increase and the agreement with the independent reconstructions decreases. We suggest that the dissimilarities are mainly due to the different target seasons (annual vs. sum of summer and winter), the decreasing number of predictors available in the multiproxy reconstructions as well as increasing dating uncertainty and decreasing temporal resolution of the lake sediment record back in time. In Central Chile, the

differences may also be due to the different calibration data (instrumental station vs. grid) and calibration periods.

#### 4. Conclusions and Outlook

[10] This study represents the first near-continental-scale seasonal precipitation reconstruction within the Southern Hemisphere. Verification statistics and comparison with independent, local datasets indicate that the currently available proxy network allows reasonably assessing variations of large-scale precipitation variability well beyond the 20th century and over wide areas of SSA. The skill of our reconstructions is highest in regions with significant amounts of precipitation falling in the respective seasons and where the coverage with proxy data is high. Some regions, including the most densely populated area of SSA in the north-east, are still very sparsely covered with proxy data, mainly before 1850. This underlines the need for more high resolution proxy data from SSA. Our reconstructions, together with new temperature [*Neukom et al.*, 2010] and circulation reconstructions, may help to improve our understanding of the influences of atmospheric and oceanic circulation patterns on SSA climate, which again can serve as a base for detection and attribution studies in the area. The multi-centennial moistening trend in austral summer and drying trend in winter towards present represent significant changes to the seasonal cycle and South American climatology. Assessment of societal and economic changes in SSA related to these changes will require further inves-

tigation. Faced with a changing climate, limited resources, and a growing population, a long-term baseline and assessment of seasonal, spatial, and temporal changes, such as provided by these reconstructions, may be useful to help refine or develop water-allocation agreements.

[11] **Acknowledgments.** RN is supported by the Swiss NSF through the NCCR Climate. JL acknowledges support by the EU/FP6 integrated project CIRCE (Climate Change and Impact Research: the Mediterranean Environment; #036961), from the EU/FP7 project ACQWA (Assessing Climate Impacts on the Quantity and Quality of Water, #212250) and from the DFG Project PRIME (PRecipitation In the past Millennium in Europe) within the Priority Program 'INTERDYNAMIK'. We thank Mariano Masiokas and Eduardo Piovano for providing their data. Many thanks go to all contributors of proxy data and to PAGES for supporting the initiative LOTRED South America. The reviewers made useful comments and suggestions and helped to improve the quality of this study.

## References

- Boninsegna, J. A., et al. (2009), Dendroclimatological reconstructions in South America: A review, *Palaeogeogr. Palaeoclimatol. Palaeoecol.*, *281*, 210–228, doi:10.1016/j.palaeo.2009.07.020.
- Cook, E. R., et al. (2004), Long-term aridity changes in the western United States, *Science*, *306*, 1015–1018, doi:10.1126/science.1102586.
- Cook, E. R., et al. (2010), Asian monsoon failure and megadrought during the last millennium, *Science*, *328*, 486–489, doi:10.1126/science.1185188.
- Frank, D., J. Esper, and E. R. Cook (2007), Adjustment for proxy number and coherence in a large-scale temperature reconstruction, *Geophys. Res. Lett.*, *34*, L16709, doi:10.1029/2007GL030571.
- Frank, D., et al. (2010), Ensemble reconstruction constraints of the global carbon cycle sensitivity to climate, *Nature*, *463*, 527–530, doi:10.1038/nature08769.
- Garreaud, R. D., et al. (2009), Present-day South American climate, *Palaeogeogr. Palaeoclimatol. Palaeoecol.*, *281*, 180–195, doi:10.1016/j.palaeo.2007.10.032.
- Jansen, E., et al. (2007), Palaeoclimate, in *Climate Change 2007: The Physical Science Basis. Contribution of Working Group I to the Fourth Assessment Report of the Intergovernmental Panel on Climate Change*, edited by S. Solomon et al., pp. 433–497, Cambridge Univ. Press, Cambridge, U. K.
- Jones, P. D., et al. (2009), High-resolution palaeoclimatology of the last millennium: A review of current status and future prospects, *Holocene*, *19*, 3–49, doi:10.1177/0959683608089852.
- Küttel, M., et al. (2010), The importance of ship log data: Reconstructing North Atlantic, European and Mediterranean sea level pressure fields back to 1750, *Clim. Dyn.*, *34*, 1115–1128, doi:10.1007/s00382-009-0577-9.
- Le Quesne, C., et al. (2009), Long-term glacier variations in the Central Andes of Argentina and Chile, inferred from historical records and tree-ring reconstructed precipitation, *Palaeogeogr. Palaeoclimatol. Palaeoecol.*, *281*, 334–344, doi:10.1016/j.palaeo.2008.01.039.
- Luterbacher, J., et al. (2002), Reconstruction of sea level pressure fields over the eastern North Atlantic and Europe back to 1500, *Clim. Dyn.*, *18*, 545–561.
- Luterbacher, J., et al. (2004), European seasonal and annual temperature variability, trends, and extremes since 1500, *Science*, *303*, 1499–1503, doi:10.1126/science.1093877.
- Magrin, G., et al. (2007), Latin America, in *Climate Change 2007: Impacts, Adaptation and Vulnerability. Contribution of Working Group II to the Fourth Assessment Report of the Intergovernmental Panel on Climate Change*, edited by M. L. Parry et al., pp. 581–615, Cambridge Univ. Press, Cambridge, U. K.
- Mitchell, T. D., and P. D. Jones (2005), An improved method of constructing a database of monthly climate observations and associated high-resolution grids, *Int. J. Climatol.*, *25*, 693–712, doi:10.1002/joc.1181.
- Moy, C. M., et al. (2009), Climate change in southern South America during the last two millennia, in *Past Climate Variability in South America and Surrounding Regions*, edited by F. Vimeux et al., pp. 353–393, doi:10.1007/978-90-481-2672-9\_15, Springer, New York.
- Neukom, R., M. del Rosario Prieto, R. Moyano, J. Luterbacher, C. Pfister, R. Villalba, P. D. Jones, and H. Wanner (2009), An extended network of documentary data from South America and its potential for quantitative precipitation reconstructions back to the 16th century, *Geophys. Res. Lett.*, *36*, L12703, doi:10.1029/2009GL038351.
- Neukom, R., et al. (2010), Multiproxy summer and winter surface air temperature field reconstructions for southern South America covering the past centuries, *Clim. Dyn.*, doi:10.1007/s00382-010-0793-3.
- Pauling, A., et al. (2006), Five hundred years of gridded high-resolution precipitation reconstructions over Europe and the connection to large-scale circulation, *Clim. Dyn.*, *26*, 387–405, doi:10.1007/s00382-005-0090-8.
- Peterson, T. C., and R. S. Vose (1997), An overview of the global historical climatology network temperature database, *Bull. Am. Meteorol. Soc.*, *78*, 2837–2849, doi:10.1175/1520-0477(1997)078<2837:A00TGH>2.0.CO;2.
- Piovano, E. L., et al. (2009), Hydrological variability in South America below the Tropic of Capricorn (Pampas and Patagonia, Argentina) during the last 13.0 Ka, in *Past Climate Variability in South America and Surrounding Regions*, edited by F. Vimeux et al., pp. 323–351, doi:10.1007/978-90-481-2672-9\_14, Springer, New York.
- Rutherford, S., et al. (2005), Proxy-based Northern Hemisphere surface temperature reconstructions: Sensitivity to method, predictor network, target season, and target domain, *J. Clim.*, *18*, 2308–2329, doi:10.1175/JCLI3351.1.
- Scherrer, S. C., and C. Appenzeller (2006), Swiss Alpine snow pack variability: Major patterns and links to local climate and large-scale flow, *Clim. Res.*, *32*, 187–199, doi:10.3354/cr032187.
- Smerdon, J. E., et al. (2010), A pseudoproxy evaluation of the CCA and RegEM methods for reconstructing climate fields of the last millennium, *J. Clim.*, doi:10.1175/2010JCLI3328.1, in press.
- van der Schrier, G., et al. (2007), Exploring an ensemble approach to estimating skill in multiproxy palaeoclimate reconstructions, *Holocene*, *17*, 119–129, doi:10.1177/0959683607073294.
- Villalba, R., et al. (1997), Sea-level pressure variability around Antarctica since AD 1750 inferred from subantarctic tree-ring records, *Clim. Dyn.*, *13*, 375–390, doi:10.1007/s003820050172.
- Wahl, E. R., and C. M. Ammann (2007), Robustness of the Mann, Bradley, Hughes reconstruction of Northern Hemisphere surface temperatures: Examination of criticisms based on the nature and processing of proxy climate evidence, *Clim. Change*, *85*, 33–69, doi:10.1007/s10584-006-9105-7.
- Wilson, R., et al. (2010), Reconstructing ENSO: The influence of method, proxy data, climate forcing and teleconnections, *J. Quat. Sci.*, *25*, 62–78, doi:10.1002/jqs.1297.
- Xoplaki, E., J. Luterbacher, H. Paeth, D. Dietrich, N. Steiner, M. Grosjean, and H. Wanner (2005), European spring and autumn temperature variability and change of extremes over the last half millennium, *Geophys. Res. Lett.*, *32*, L15713, doi:10.1029/2005GL023424.

J. Esper, Department of Geography, Johannes Gutenberg University, D-55099 Mainz, Germany.

D. Frank, Swiss Federal Research Institute WSL, Zürcherstrasse 111, CH-8903 Birmensdorf, Switzerland.

M. Grosjean, R. Neukom, and H. Wanner, Institute of Geography, Climatology and Meteorology, University of Bern, Hallerstrasse 12, CH-3012 Bern, Switzerland. (neukom@giub.unibe.ch)

P. D. Jones, Climatic Research Unit, School of Environmental Sciences, University of East Anglia, Norwich NR4 7TJ, UK.

M. Küttel, Department of Earth and Space Sciences, University of Washington, Box 351310, Seattle, WA 98195, USA.

L. Lopez and R. Villalba, Instituto Argentino de Nivología y Glaciología y Ciencias Ambientales, CONICET, Av. Dr. Adrián Ruiz Leal s/n, C.C. 330, 5500 Mendoza, Argentina.

J. Luterbacher, Department of Geography, Climatology, Climate Dynamics and Climate Change, Justus Liebig University Giessen, Senckenbergstrasse 1, D-35390 Giessen, Germany.

# Supplementary Material

## S1. Alternative illustrations of the reconstructions

Figure S1 shows the spatial means of the reconstructions comparing the ensemble mean and median. Figures S2-S5 show alternative (to Figure 3 in the main text) illustrations of the reconstruction ensembles.

## S2. Selection of the precipitation proxies

Out of a database of 144 proxies [Neukom *et al.*, 2010] that are related to SSA climate (e.g. temperature or precipitation), we selected the predictors with temporally stable and significant correlations with SSA summer (DJF) or winter (JJA) precipitation.

As a first selection criterion we used the absolute Spearman correlation of the proxies with the 20<sup>th</sup> century instrumental CRU TS 3 grid [updated from Mitchell and Jones, 2005] in the overlapping period (between 70 and 106 years within 1901-2006). Only proxies with at least one grid cell with significant ( $p < 0.05$ ) correlation were considered for the further analyses. The grid cell with the highest absolute correlation was defined as “best location” for the proxy. The maximum correlations and the corresponding coordinates of the “best locations” are indicated in Tables S1 (summer) and S2 (winter). We are aware that the chosen alpha-level ( $p < 0.05$ ) may lead to Type I errors in a grid of 2358 cells. However, Tables S1 and S2 show that most proxies have significant correlations over large parts of the grid (mostly more than 5%) and these areas are in all cases mostly formed by adjacent cells and not randomly distributed over the continent (not shown). The “best location” is in most cases in the same climatic region as the proxy itself. Exceptions can be explained by the limited quality of the instrumental grid in some areas [see e.g. Garreaud *et al.*, 2009; Neukom *et al.*, 2010] and/or strong teleconnections in the region, mainly related to SAM (Southern Annular Mode) and ENSO [El Niño-Southern Oscillation; e.g. Garreaud *et al.*, 2009; Villalba, 2007; Villalba *et al.*, 1997b].

In order to test the validity and stability of these teleconnections, which is particularly important for the proxies from outside SSA, we evaluated the temporal stability of the proxies’ correlations with the “best locations”. This was evaluated by calculating 30-year running Spearman correlation coefficients between each proxy series and the corresponding instrumental grid cell. If the running correlation curve showed instabilities (i.e. changes in sign, or fluctuations in the coefficient that exceed  $\pm 0.2/\text{decade}$ ) the relation between the proxy and the predictand was considered not stable and the proxy series was excluded from the potential predictor matrix. We are aware that all selection criteria introduce some subjective pre-filtering into the reconstructions. However, due to the relatively large number of proxies used and the ensemble approach, the probability of single proxies dominating or even biasing the reconstructions is small (see section S5 and Figures S13-S16). The 33 (31) proxy series that were finally included into the predictor matrix for the austral summer (winter) precipitation reconstructions are shown in Table S1 (Table S2) and Figure 1a (Figure 1b) in the main text.

## S3. Statistical skill measures

Figure S6 shows the temporal evolution of the average correlations between all ensemble members ( $\overline{r}$ ; 30 year moving windows) as well as the average RE [Cook *et al.*, 1994] and  $r^2$  for both seasons. All values are at rather low levels ( $\overline{r}$  0.2-0.6; RE 0.09-0.12;  $r^2$  0.05-0.1) before 1851, where no instrumental predictors are available. They thereafter rapidly increase to values above 0.86 ( $\overline{r}$ ) and 0.27 (RE) and 0.28 ( $r^2$ ) in both seasons.

Figure S7 shows the spatial distribution of the RE values, averaged over the entire reconstruction period for austral summer (left; 1498-1995) and winter (right; 1590-1995). The highest skill is found over central Chile and central-eastern SSA in summer and over central

to northern Chile and west-central Argentina in winter. The lowest REs are found in northern- and southernmost SSA in both seasons. As the average REs over the ensembles are relatively low, we evaluated the influence of ensemble members of different REs on the ensemble distribution and median. Figures S8 and S9 show that the ensemble median remains remarkably stable if all members, only the members with positive REs, or only the one percent (i.e. 100 members) with the highest RE scores are selected. The Spearman Correlations between the medians of the three subsets are all greater than 0.994 in both seasons. The differences between the three median curves are not only small (mostly less than  $\pm 0.1$  standard deviations) but the residuals also follow (though statically not-significant) a normal distribution (Figures S8 and S9 lower panels). Figures S10 and S11 show that the 100 best ensembles (based on RE) are much narrower distributed than the entire set or a random selection of 100 ensembles but, as shown above, with practically the same median. These figures provide evidence that the final reconstruction (the ensemble median) is robust, relatively skilful and not biased by unreliable ensemble members. It must be noted the RE statistics are based on varying calibration/verification intervals (as they were sampled for each ensemble member). Hence varying RE values are not only caused by changes in the proxy network and PC-truncations, but also by the different calibration/verification intervals.

We also assessed the quality of the final reconstruction (ensemble median) in the period of instrumental overlap (1931-1995). The Root mean squared error of Prediction (RMSEP) and explained variance ( $r^2$ ) of the target are shown for each grid cell in Figure S12. The average RMSEP over SSA is 0.67 (0.65) std. dev. for summer (winter), the average  $r^2$  over SSA is 0.60 for summer and 0.61 for winter. These results are positively biased, as the period considered encloses the (varying) calibration periods of all ensemble members. Also here, the best measures (low RMSEP and high  $r^2$ ) can be found in the central part of SSA whereas in the very north and south, the skill is lower.

Overall, the regions with high regression skill (RE, RMSEP and  $r^2$ ) and low uncertainties (see Figure 2 in the main text) are primarily the Chilean part of northern Patagonia (ca. 37°S-45°S) in summer, and Chile between 28°S and 45°S as well as central SSA in winter. For both seasons, the lowest skill and highest uncertainties broadly coincide with regions where precipitation is low (see Figure 1). The reduced reliability in the peripheral areas of SSA is probably due to the limited quality of the instrumental grid in these regions [Garreaud *et al.*, 2009; Neukom *et al.*, 2010] and the smaller number of proxies available (Figure 1).

Finally, it must be noted that all quality measures provided are likely positively biased by the inclusion of the instrumental predictors, which had mostly also been included into the calculation of the calibration grid. However, as described in section S5 and shown in Figures S17 and S18, the reconstruction itself does in most areas not significantly change by the inclusion of instrumental predictors.

#### **S4. Methodological details on the comparison plots (Figures 3c and 3d in the main text)**

As an additional validation, we compared our (30-year filtered) reconstructions with independent regional moisture reconstructions in SSA (Figures 3c and 3d in the main text). Figure 3c shows our reconstruction in the catchment area of the Laguna Mar Chiquita in northern Argentina (30°54'S/62°51'W) along with the lake level reconstruction by Piovano *et al.* [2009]. Our reconstruction is shown as the percentiles of the DJF+JJA sum, which explains 63% of annual precipitation variability in the instrumental data (CRU TS 3 grid 1931-1995) in this area. The curve of the Piovano *et al.* [2009] lake level reconstruction (black) is derived as follows: We only use the fraction of the reconstruction [Figure 14.3 in Piovano *et al.*, 2009] that goes back to 1770, as before this date, the temporal resolution decreases considerably. There are four dated points in this interval [1770, 1803, 1900 and 1976; Piovano *et al.*, 2009; green points in Figure 3c]. We derived the ages of the other points

(black points in Figure 3c) by linear interpolation. The lake level is indicated in meters relative to the 1976-1977 shoreline [Piovano *et al.*, 2009].

Figure 3d shows a regional reconstruction comparison in Central Chile. The black curve represents the precipitation reconstruction of Le Quesne *et al.* [2009] which is exclusively based on tree rings. It was calibrated in the period 1866-1999 using the instrumental station “Quinta Normal” at Santiago de Chile [Le Quesne *et al.*, 2009]. The thin black to red lines show the percentiles our DJF+JJA reconstruction in Central Chile (30°S-35°S / 70°W-72°W; an area covering Santiago de Chile and surroundings as well as the tree ring sites used by Le Quesne *et al.* [2009]). In this area, 78% of annual precipitation variability explained by the DJF+JJA sum in CRU TS 3. These two reconstructions are not fully independent because some (65 out of 117) of the tree ring samples included in one of the three sites used as predictors by Le Quesne *et al.* [2009] are also part of the “El Asiento” record used in this study (Table S2). However, regarding the total number of tree ring samples and overall predictors used in both studies, this overlap is very marginal (the overlapping samples represent 56% of the tree ring series in Le Quesne *et al.* [2009] and 5.6% of the tree ring samples used herein, which, in turn, represent 22% of the total number of predictors used).

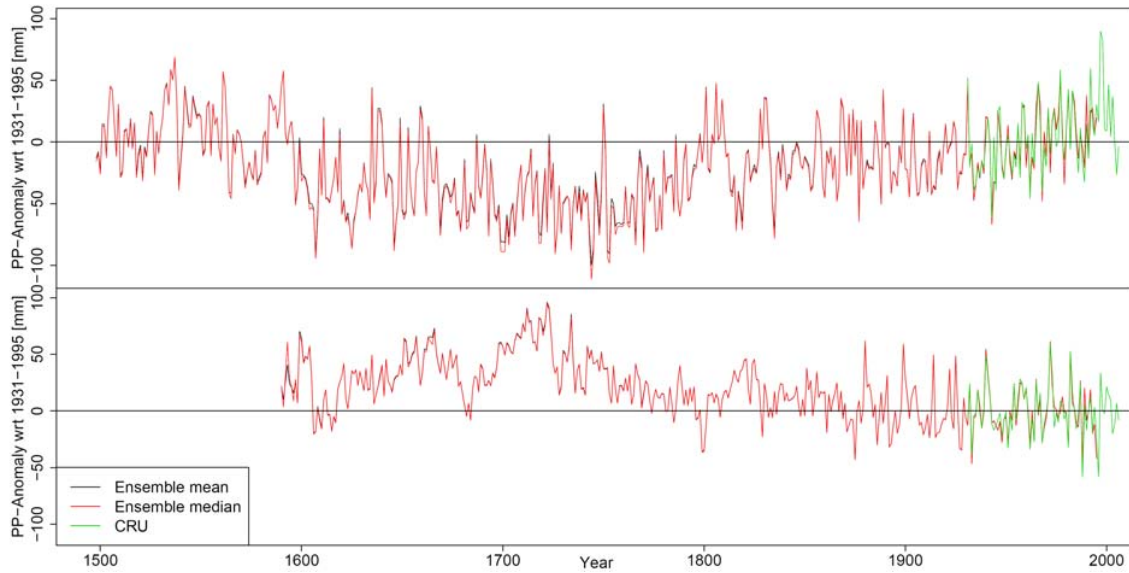
### **S5. Regression weights of the predictors and importance of the instrumental predictors**

In order to investigate whether our reconstructions are strongly dependent on single predictors, the weight that each predictor has at each time step and location in our regression models was calculated [see e.g. Briffa *et al.*, 1986]. The calculations are based on a single reconstruction using the following settings:

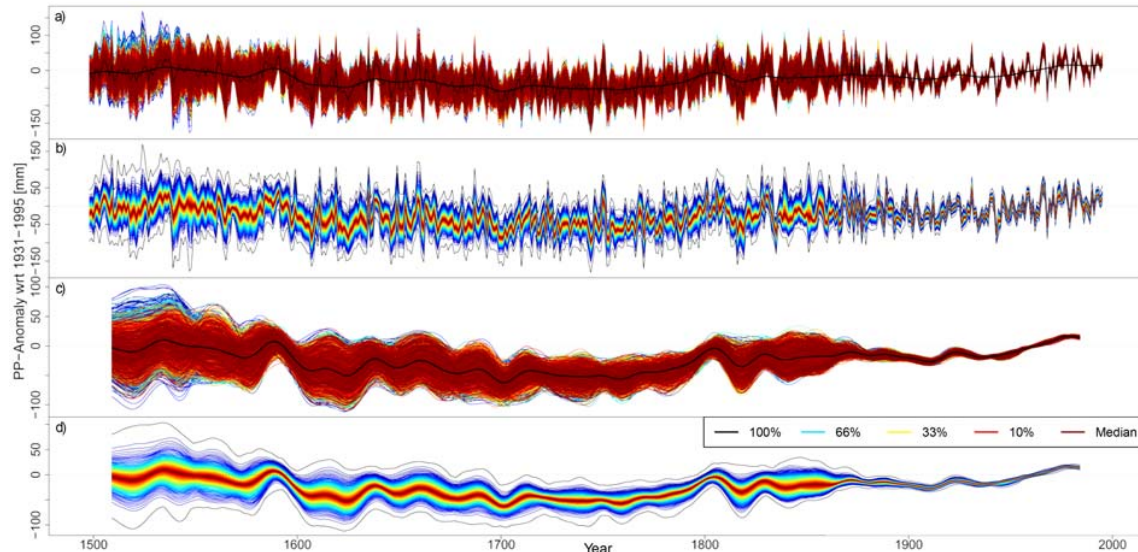
We included all predictors (Tables S1 and S2), used 1931-1995 as calibration period and retained the first  $n$  principal components explaining 90 (80) percent of the total variance in the predictor (instrumental) matrix. In order to deal with the changing number of predictors over time, the sum of the weights was normalized to a value of one at each year and all weights were then multiplied with the number of predictors available in the respective year. The spatially averaged weight of each predictor in four selected years for austral summer (winter) is shown in Figure S13 (S15) and Table S1 (S2). The predictors with the largest weight at each location in the same years are displayed in Figure S14 (S16). These Figures indicate that our reconstructions are not dominated by single predictors.

Figure S17 displays the spatial average of our summer and winter reconstructions together with the same reconstruction based on non-instrumental predictors only (after 1851, when the first instrumental series starts). Figure S18 shows the spatial correlation between these two reconstructions. The two reconstructions are within the uncertainty bands of each other, except for a few years in winter around 1910. There are some areas where the instrumental predictors have a strong influence on the outcome of the reconstructions: most of Patagonia in summer and north-western Patagonia, north-central SSA as well as, most clearly, the province of Buenos Aires in winter. In these areas, the reconstructions must be interpreted with caution before 1851, when the first instrumental series begins.

## Figures



**Figure S1:** Spatial anomaly mean of the austral summer (DJF; top; 1498-1995) and winter (JJA; bottom; 1590-1995) reconstructions with respect to the 1931-1995 climatology using the ensemble mean (black) and median (red) as reconstructed value, respectively. Green: CRU gridded data 1931-2006.



**Figure S2:** SSA mean austral summer precipitation reconstruction ensemble 1498-1995 relative to the 1931-1995 climatology. a) Interannual reconstruction anomalies. Blue to red lines: ensemble members. Black: ensemble median. Bold black: 30-year Gaussian filtered ensemble median. b) Percentiles of the reconstruction ensemble. Each line represents a percentile. The area between the black lines encloses all (100%) members; the area between the lowest blue line (1<sup>st</sup> percentile) and the highest blue line (99<sup>th</sup> percentile) blue lines encloses 98% of the members, and so on. c) and d) Same as a) and b) but for the 30-year Gaussian filtered ensemble members.

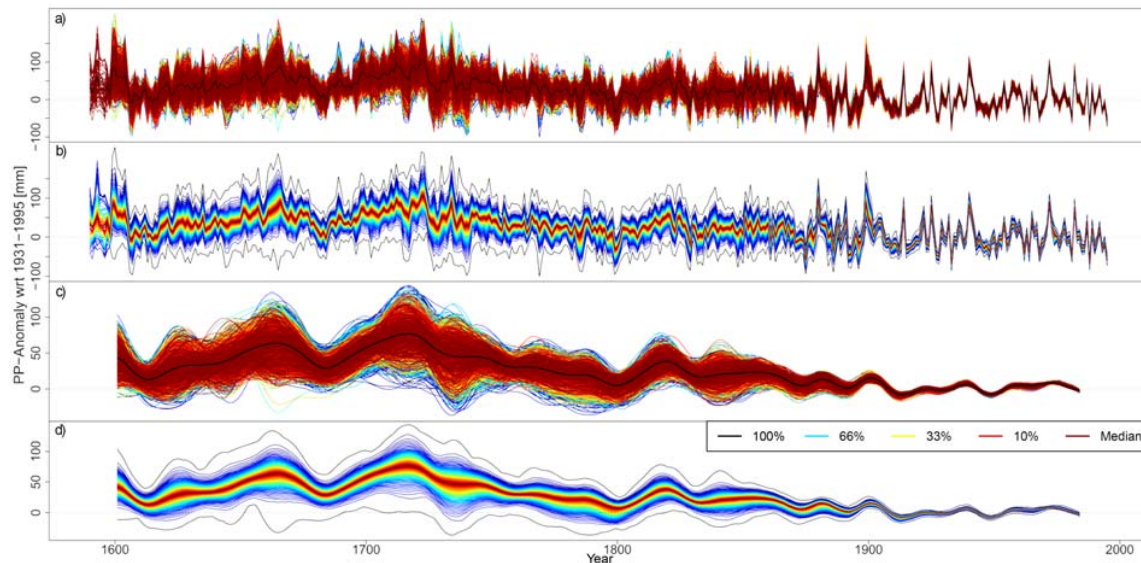


**Figure S3:** Same as Figure S2 but for austral winter and the period 1590-1995.

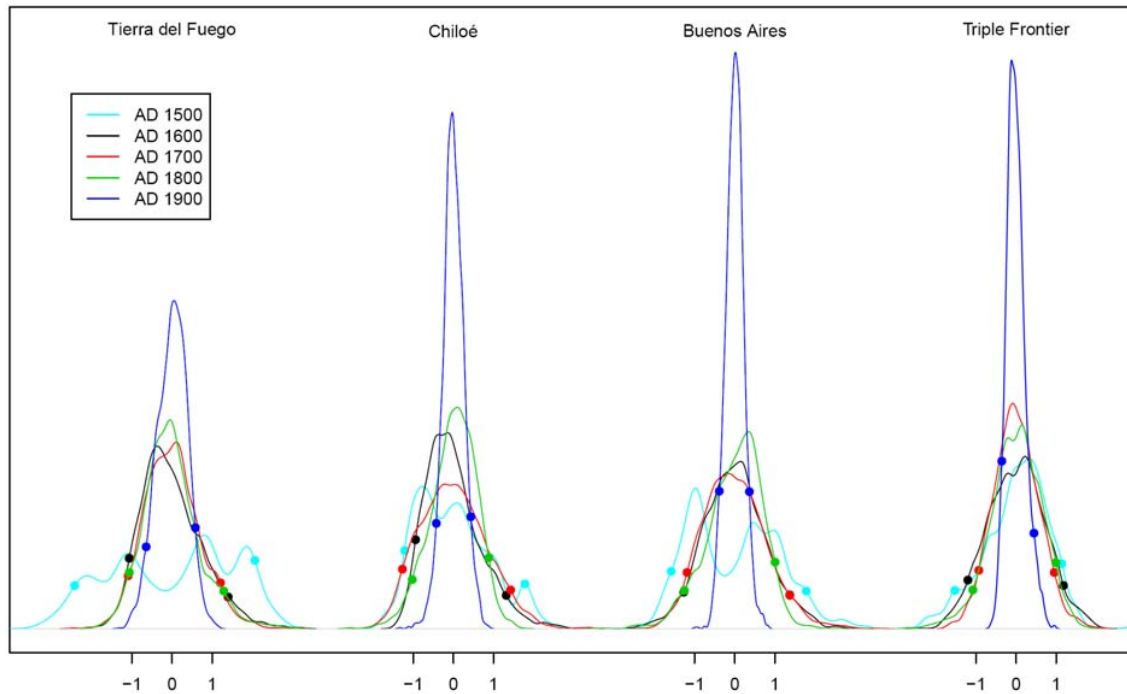


**Figure S4:** Distribution functions of the ensemble members of the summer precipitation reconstruction at four selected grid points: Tierra del Fuego ( $68^{\circ}\text{W}/54^{\circ}\text{S}$ ; left), Chiloé Island ( $74^{\circ}\text{W}/42^{\circ}\text{S}$ ; second), Buenos Aires ( $58^{\circ}\text{W}/34.5^{\circ}\text{S}$ , third) and Triple Frontier (tri-border area of Argentina, Brazil and Paraguay,  $54.5^{\circ}\text{W}/25.5^{\circ}\text{S}$ ; right). The distribution functions are shown for the years AD 1500 (turquoise), 1600 (black), 1700 (red), 1800 (green) and 1900 (blue). All curves are normalized to a mean of zero and divided by the standard deviation of precipitation (1931-1995) at each location. The coloured dots show the 5<sup>th</sup> and 95<sup>th</sup> percentiles, which were used to define the reconstruction uncertainties (see main text).

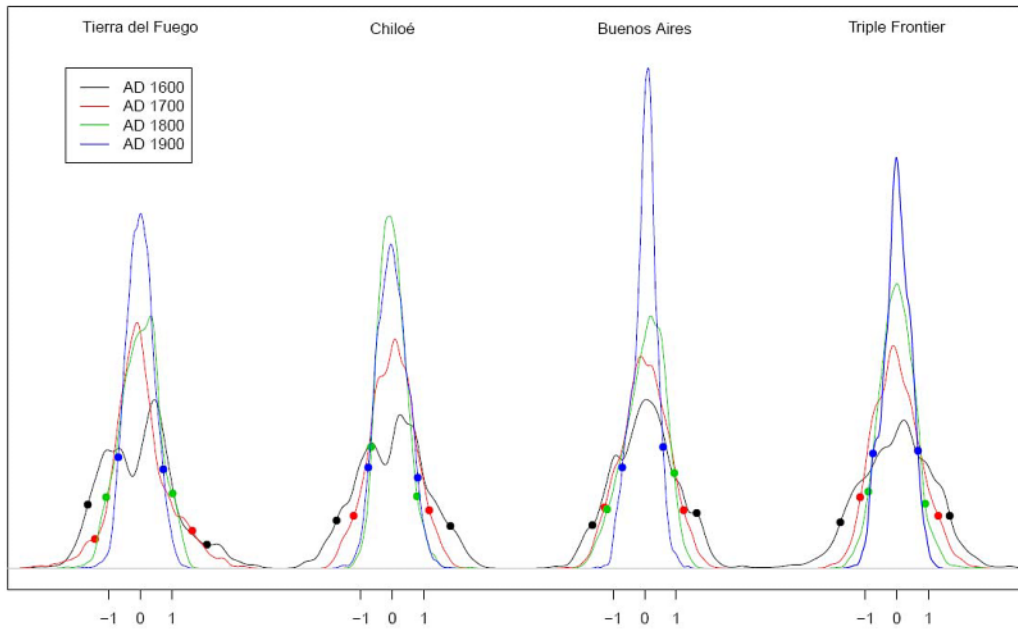


**Figure S5:** Same as Figure S1 but for winter and the years 1600, 1700, 1800 and 1900.

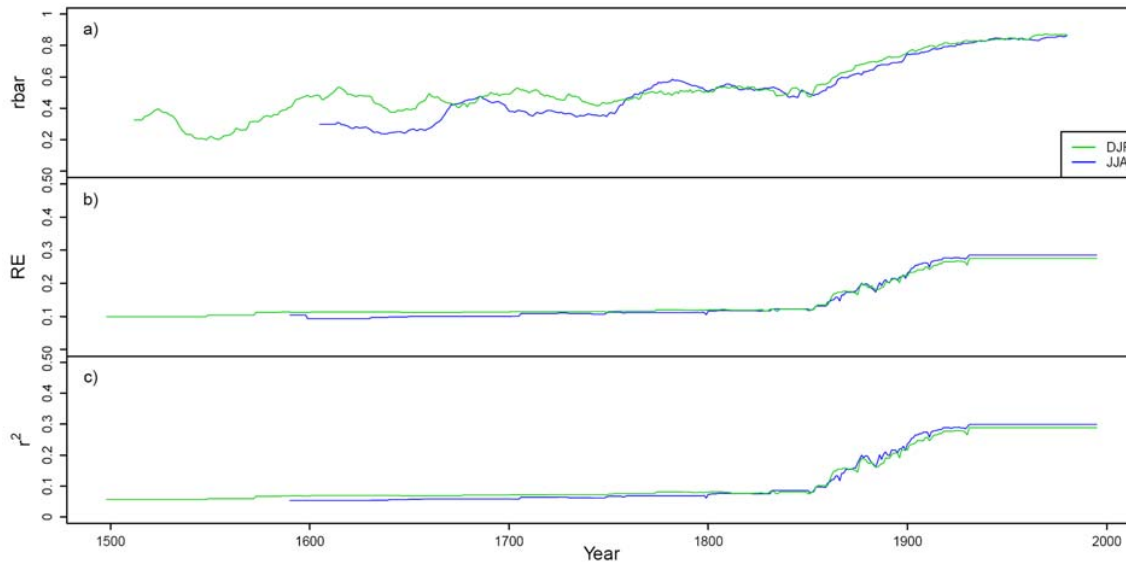


**Figure S6:** Mean 30-year running correlation between the predictor series ( $r_{bar}$ ; a) and spatial average of the ensemble mean RE (b) and  $r^2$  (c) for the austral summer (green; 1498-1995) and winter (blue; 1590-1995) reconstructions.

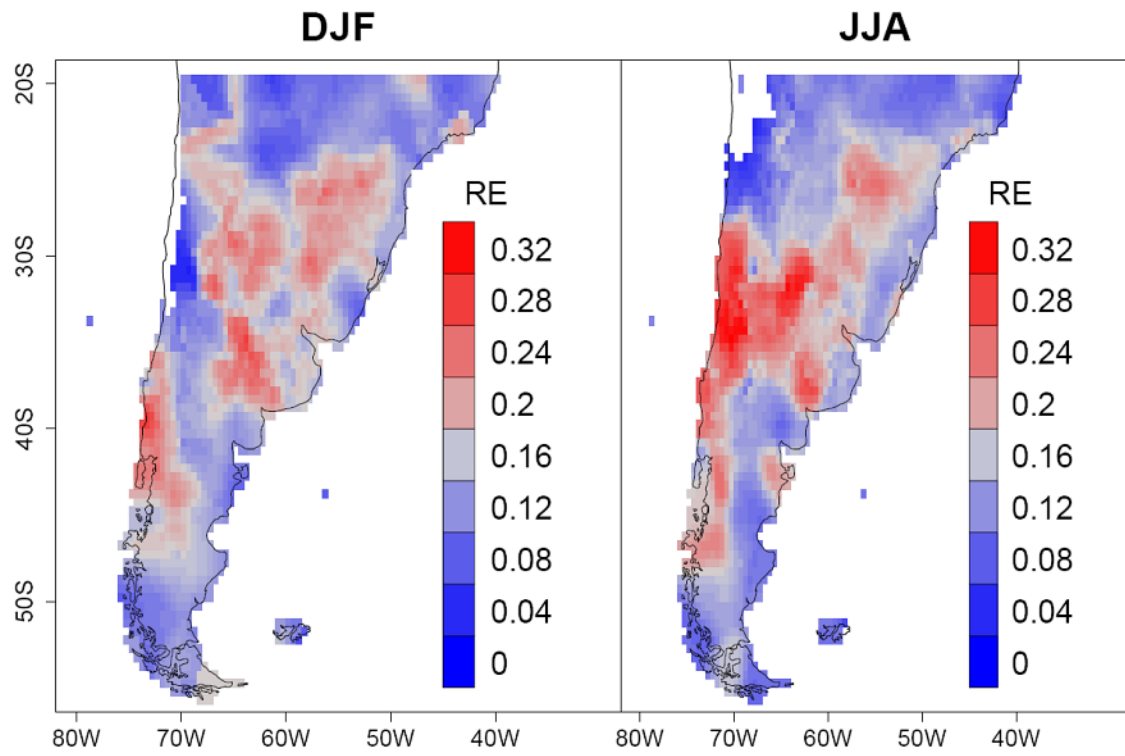


**Figure S7:** Spatial distribution of the RE values, averaged over the entire ensemble and reconstruction period for austral summer (left; 1498-1995) and winter (right; 1590-1995).

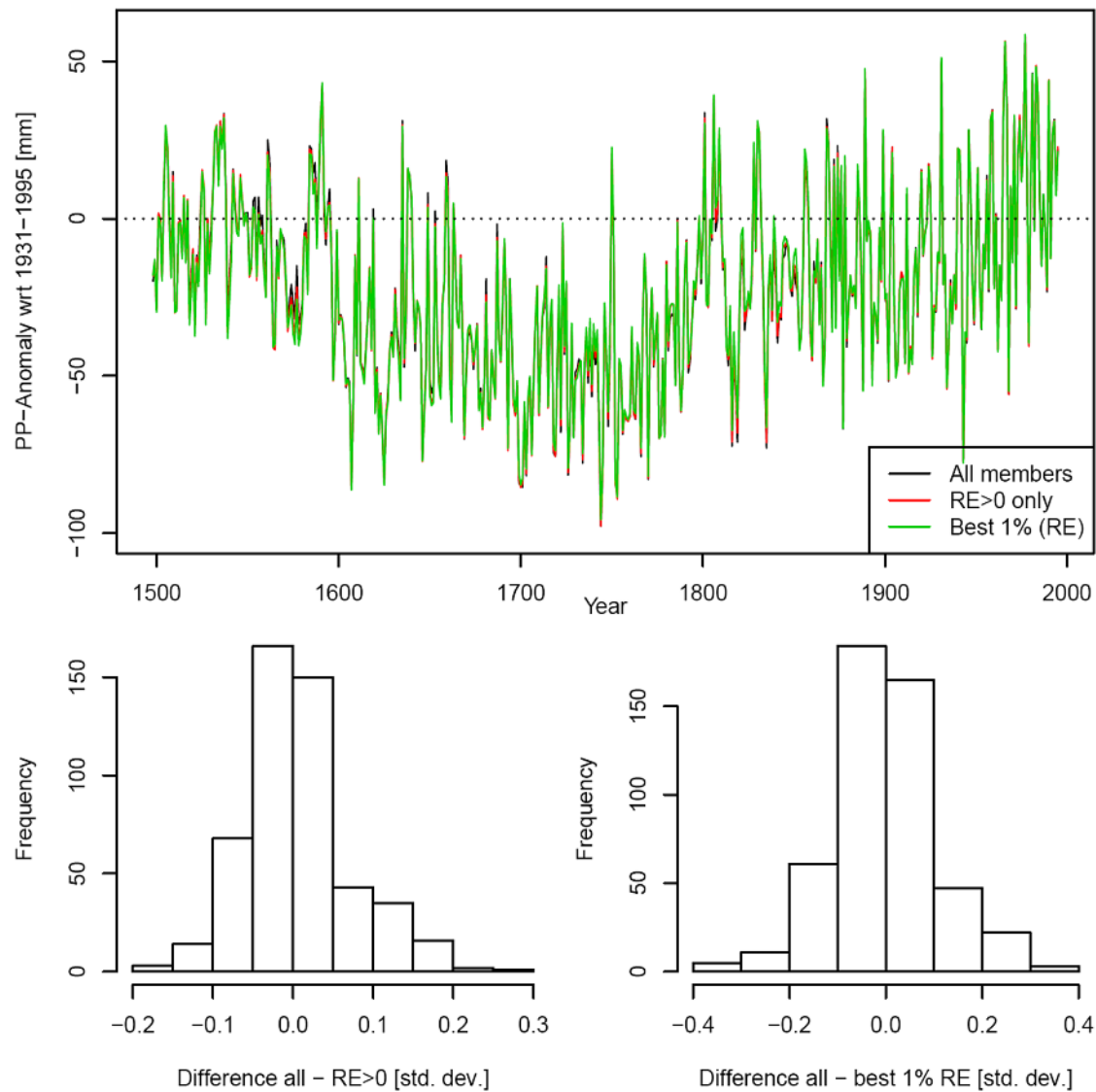


**Figure S8:** Top: Austral summer reconstruction ensemble median 1498-1995 based on all members (black), only the members with positive REs (red) and only the best percent of the members, based on the RE skills (green). Bottom: Histogram of the residuals between the median of all members and the members with positive REs only (left) and between the median of all members and the best percent of the members only (right).

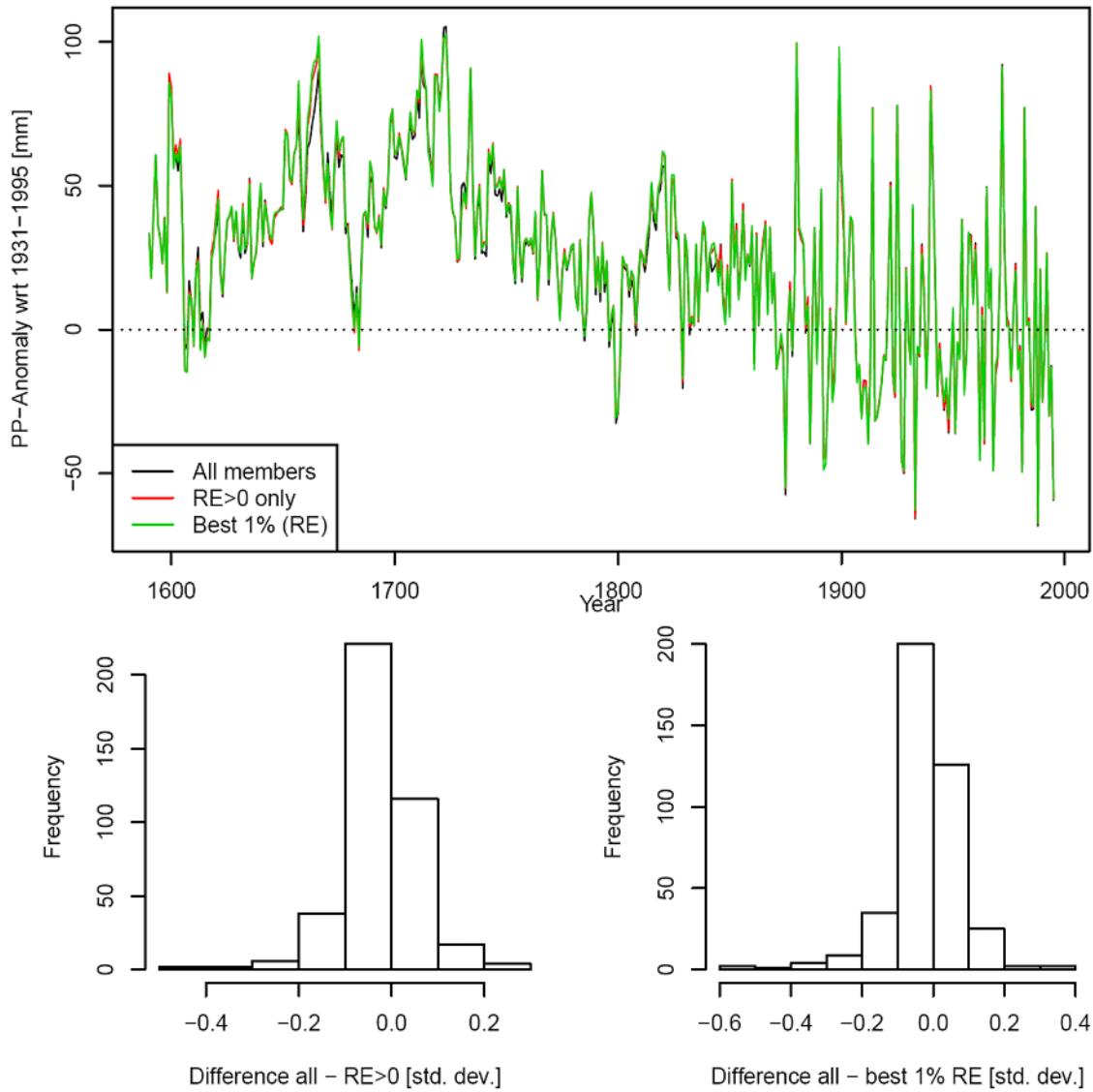


**Figure S9:** Same as Figure S8 but for austral winter and the years 1590-1995.

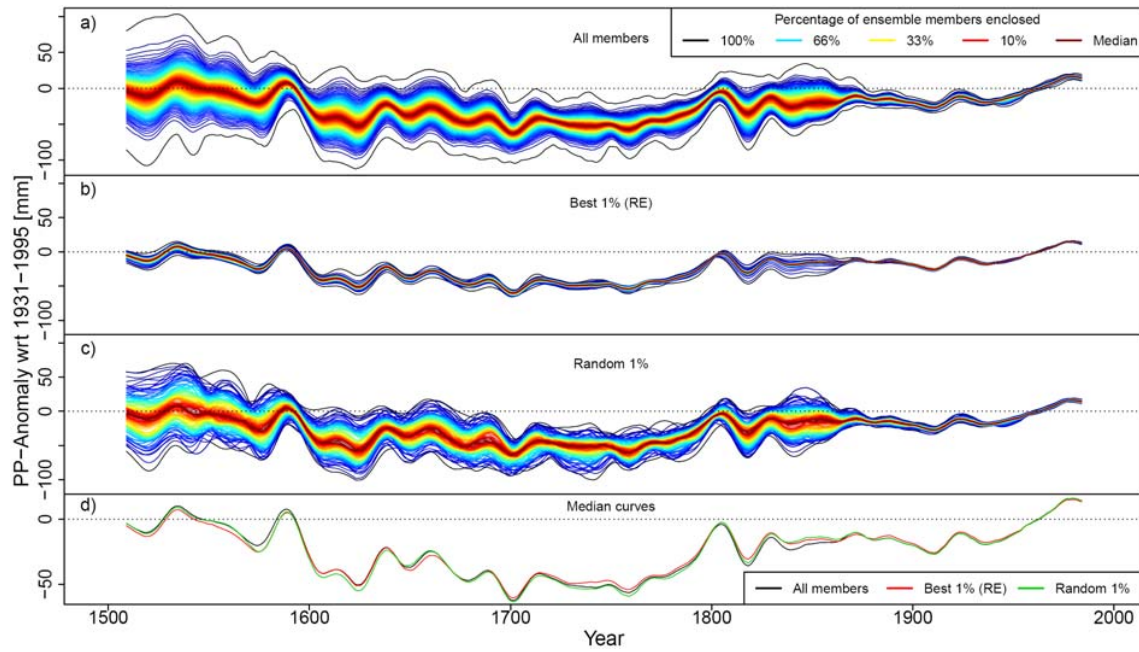


**Figure S10:** Percentiles of the ensemble member distribution of the 30-year filtered summer precipitation reconstruction 1498-1995. a) ensemble of all members; b) ensemble of the best percent of members only (based on the RE skills); c) ensemble of a random selection of 100 members (1%); d) median curves of the three ensembles.

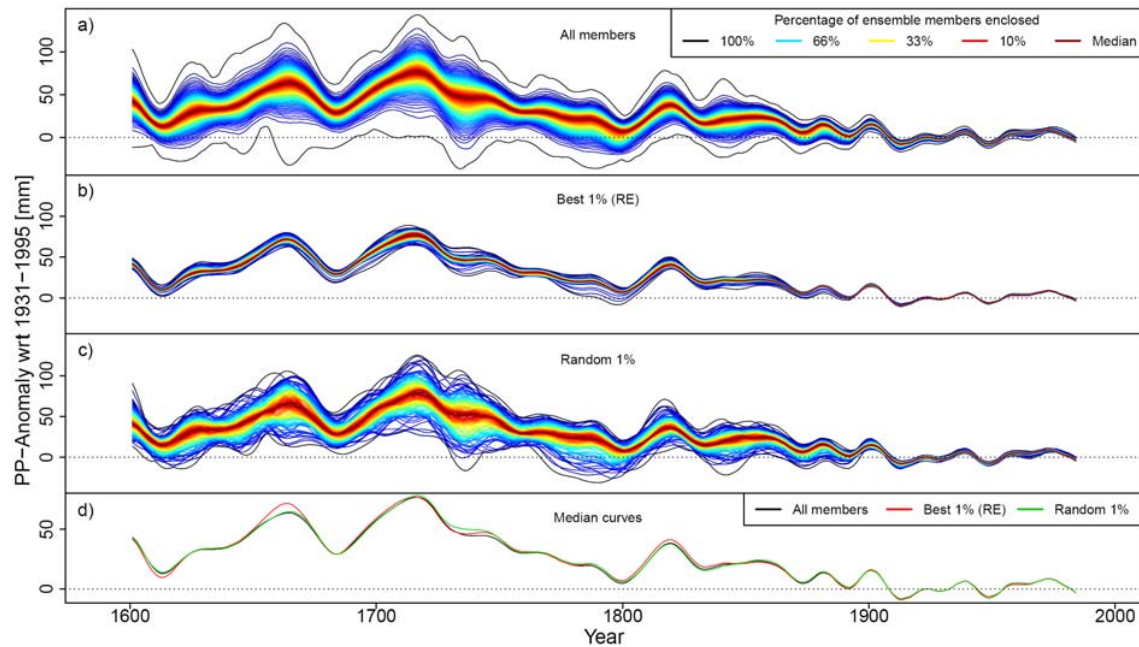


**Figure S11:** Same as Figure S10 but for austral winter and the years 1590-1995.

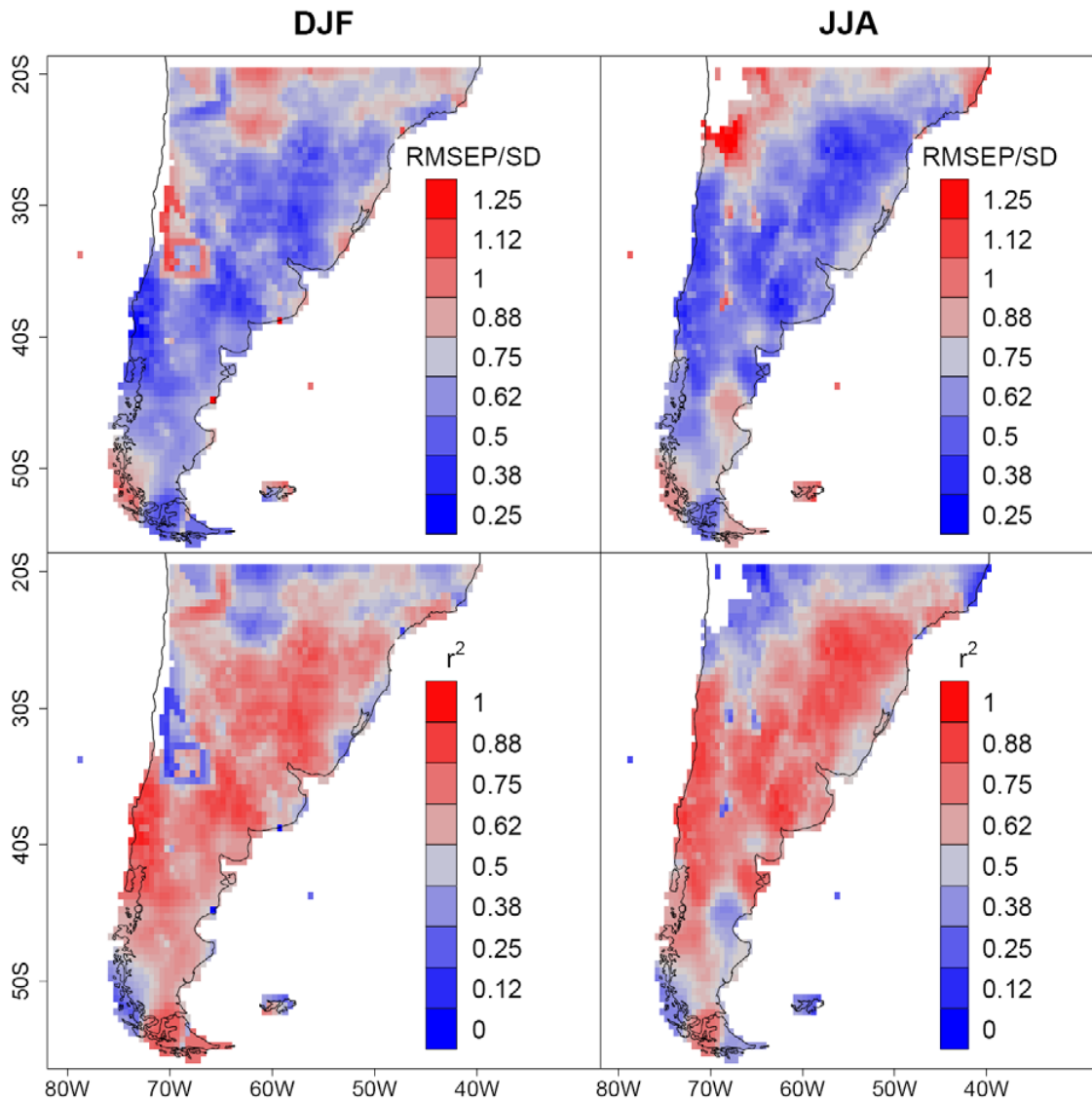


**Figure S12:** Spatial distribution of the root mean squared error of prediction (RMSEP; top) and  $r^2$  (bottom) of the reconstruction ensemble median compared with the instrumental target in the period 1931-1995. RMSEP values are relative to the instrumental standard deviation 1931-1995. Left austral summer; right austral winter.

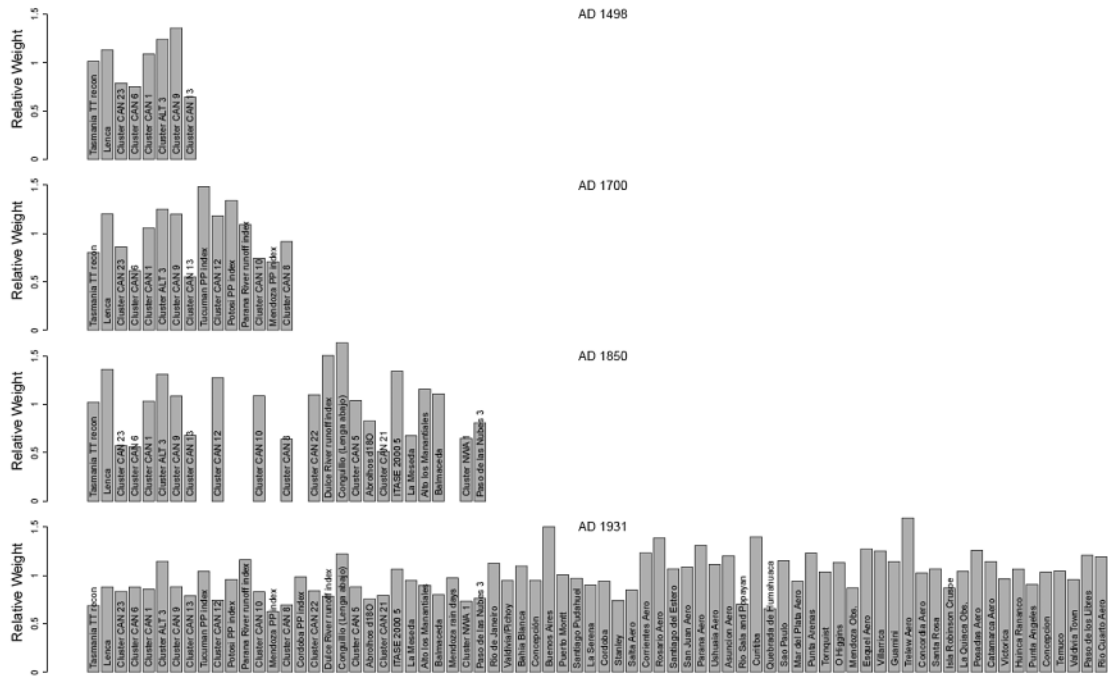


**Figure S13:** Relative, spatially averaged weight of each predictor in the summer precipitation reconstruction in the years 1498, 1700, 1850 and 1931. See also Table S1.

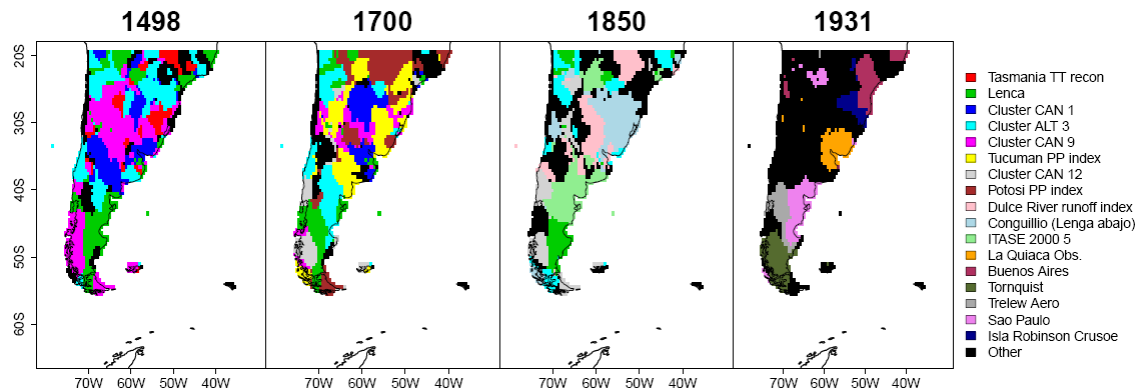


**Figure S14:** Predictor with the largest regression weight at each grid cell in the summer precipitation reconstruction in the years 1498 (first panel) 1700 (second panel) 1850 (third panel) and 1931 (last panel)

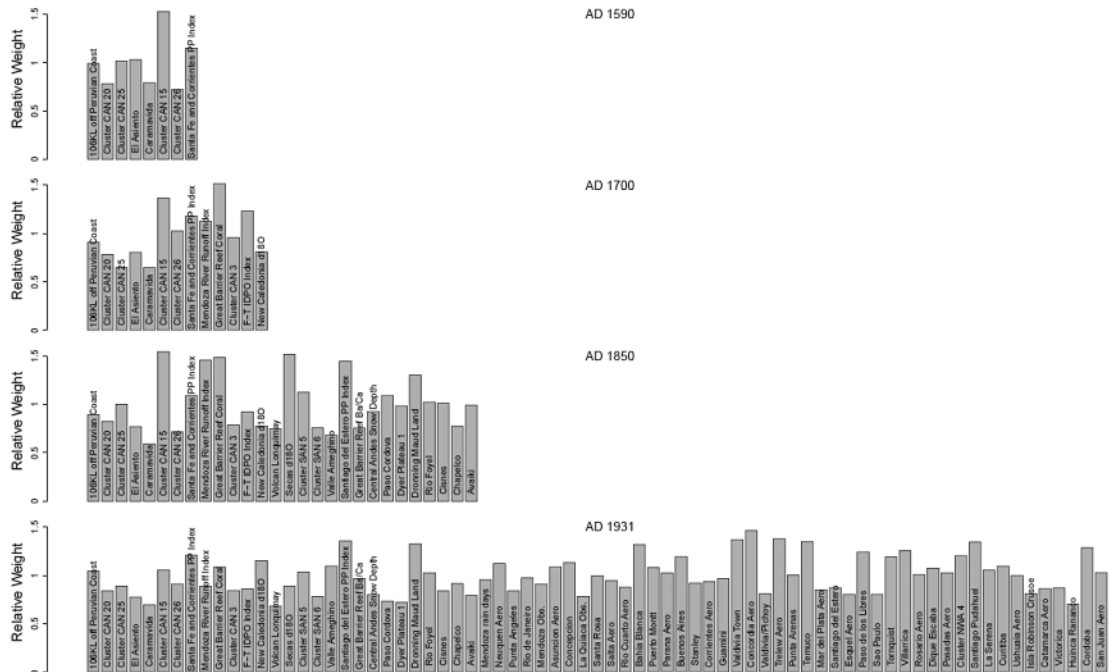


Figure S15: Same as Figure S4 but for winter and the years 1590, 1700, 1850 and 1931. See also Table S2.

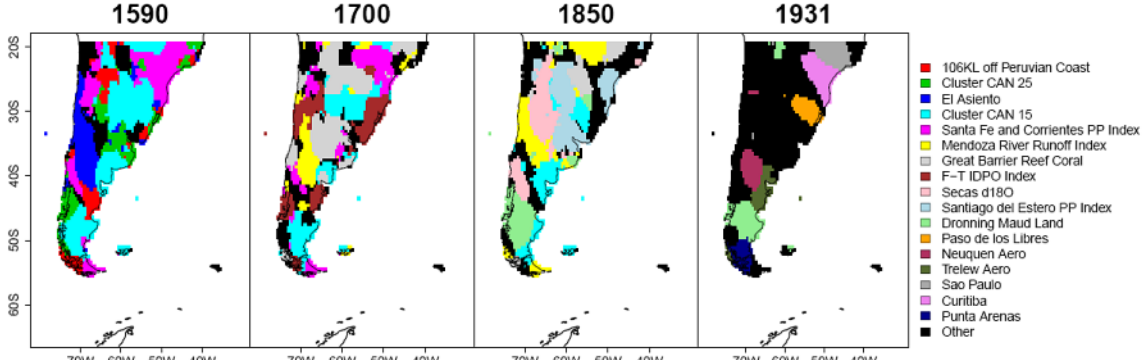
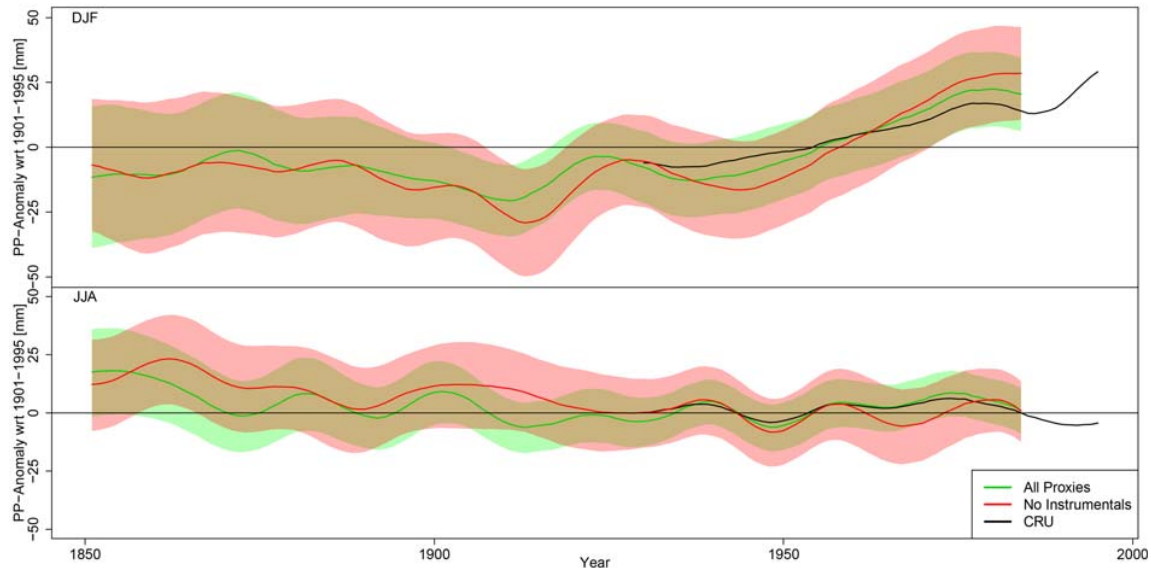
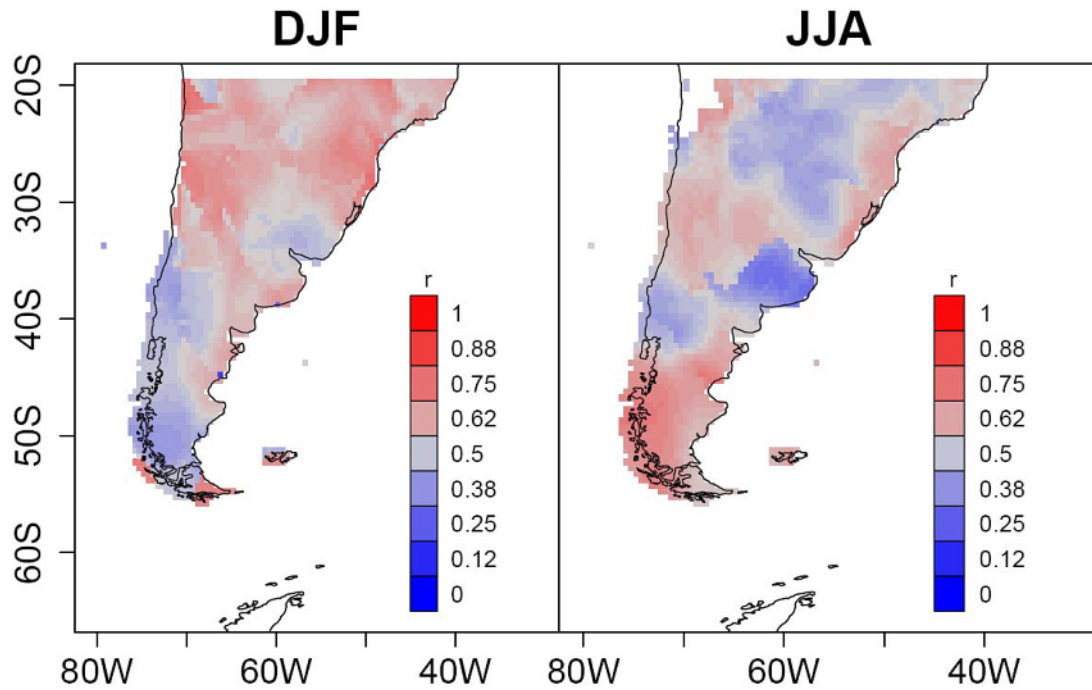


Figure S16: Same as Figure S5 but for winter and the years 1590, 1700, 1850 and 1931.



**Figure S17:** 30-year filtered austral summer (top) and winter (bottom) reconstructions based on all (green) and the non-instrumental (red) predictors 1851-1995. Filtered uncertainty bands are shaded (uncertainties are defined as the root mean squared difference between the ensemble median  $P$  and the 5<sup>th</sup> and 95<sup>th</sup> percentiles of the ensembles, respectively). Black: CRU gridded data 1931-2006.



**Figure S18:** Spatial Spearman correlation coefficients between the reconstructions based on all and only the non-instrumental predictors, respectively. Left: austral summer, right: austral winter. Period: 1851-1995. Correlations above 0.16 are significant at the 5% level (all values are significant except one grid cell in summer).

## Tables

**Table S1:** Predictors used for the austral summer (DJF) precipitation reconstructions. Start and end years are AD. The non-instrumental predictors are taken from the SSA proxy network of Neukom et al. [2010]. Columns nine to twelve quantify the Spearman correlations of the proxies with the instrumental grid 1931-1995: The highest absolute correlation (max.  $r$ ; correlation at the “best location”), the coordinates of the “best location” and the percentage of grid cells with significant ( $p < 0.05$ ) correlations. The last four columns indicate the average relative regression weight of each predictor in the years 1498, 1700, 1850 and 1931, respectively (see also Figure S13). Notice that some of the documentary and early instrumental data have missing values in 1850.

Nr.	Name	Archive	Start	End	Lon W	Lat S	Reference	Correlation with instr. Gridboxes				Proxy Weight			
								max. $r$	Lon W	Lat S	% $p < 0.05$	1498	1700	1850	1931
1	Tasmania temperature reconstruction	Tree rings	-1600	1991	-148	43	Cook et al. [2000]	0.42	58	37.5	20	1.01	0.8	1.02	0.69
2	Lenca	Tree rings	-499	1987	72.6	41.6	Lara and Villalba [1993]	-0.37	69	23.5	6	1.13	1.2	1.36	0.88
3	Cluster CAN 23	Tree rings	799	1993	71.83	42	Lara et al. [2000]	-0.38	47	20.5	8	0.78	0.86	0.57	0.83
4	Cluster CAN 6	Tree rings	1232	1983	71.5	38.5	La Marche et al. [1979a; 1979b]; Villalba [1990a]	-0.32	68	32.5	3	0.75	0.61	0.56	0.88
5	Cluster CAN 1	Tree rings	1276	1975	70.5	34.5	La Marche et al. [1979b]	0.47	57.5	27	15	1.09	1.06	1.03	0.85
6	Cluster ALT 3	Tree rings	1399	2003	67.5	21.5	Argollo et al. [2004]; Soliz et al. [2009]; Morales et al. [2004]	0.46	69.5	24.5	9	1.24	1.25	1.31	1.15
7	Cluster CAN 9	Tree rings	1407	1989	71.25	39.3	La Marche et al. [1979a]	-0.48	65	30	26	1.36	1.2	1.09	0.88
8	Cluster CAN 13	Tree rings	1498	2003	71.25	41	La Marche et al. [1979a]; Lara et al. [2008]; Villalba and Veblen [1997]	0.4	71	41.5	5	0.64	0.55	0.68	0.79
9	Tucuman precipitation index	Documentary	1548	1810	65	27	Prieto et al. [2000]; Neukom et al. [2009]	0.44	67.5	30	18	1.48			1.04
10	Cluster CAN 12	Tree rings	1572	1992	71	40	Villalba and Veblen [1997]; La Marche et al. [1979b]	-0.49	67	25.5	32	1.18	1.27	0.74	
11	Potosi precipitation index	Documentary	1585	1814	65.75	19.6	Gioda and Prieto [ <i>Gioda and Prieto</i> , 1999a; 1999b]; Neukom et al. [2009]	0.5	65	20.5	11	1.34			0.96
12	Parana River runoff index	Documentary	1590	1805	60	30	Prieto [ <i>Prieto</i> , 2007]; Neukom et al. [2009]	0.36	56	27.5	6	1.09			1.16
13	Cluster CAN 10	Tree rings	1596	1989	70.83	39.5	La Marche et al. [1979a]; Villalba and Veblen [1997]	-0.41	47.5	20.5	5	0.74	1.09	0.83	
14	Mendoza precipitation index	Documentary	1600	1810	68	32	Prieto et al. [2000]; Neukom et al. [2009]	0.56	68	32.5	11	0.71			0.63
15	Cluster CAN 8	Tree rings	1676	1989	71.17	39.2	Villalba and Veblen [1997]	0.5	51	24.5	16	0.92	0.64	0.7	
16	Cordoba precipitation index	Documentary	1701	1803	64	31	Prieto and Herrera [2001]; Neukom et al. [2009]	0.37	66	31.5	8				0.98
17	Cluster CAN 22	Tree rings	1720	1997	71.75	41.8	Villalba et al. [1998]; Schmelter [2000]	0.38	75	44.5	6			1.1	0.84
18	Dulce River runoff index	Documentary	1750	1921	65	27	Herrera et al. [2003]; Neukom et al. [2009]	-0.48	69.5	24	27			1.5	0.79
19	Conguillio (Lenga abajo)	Tree rings	1774	1996	71.6	38.6	Lara et al. [2001]	0.53	56	29.5	22			1.64	1.22

20	Cluster CAN 5	Tree rings	1787	1996	71.58	38.6	Lara et al. [2001]	-0.39	49	26	8	1.04	0.88
21	Abrolhos d <sup>18</sup> O	Corals	1794	1993	-114	28.5	Kuhnert et al. [1999]	0.36	73.5	39.5	9	0.83	0.76
22	Cluster CAN 21	Tree rings	1796	1989	71.5	41.5	Villalba and Veblen [1997]	-0.37	67.5	32	6	0.52	0.79
23	ITASE 2000 5	Ice Cores	1800	1999	124	77.7	Schneider et al. [2006]	-0.52	69	42	17	1.34	1.06
24	La Meseda	Tree rings	1826	1999	65.02	23	Unpublished	0.48	66	48.5	17	0.68	0.95
25	Alto los Manantiales	Tree rings	1827	1986	69.08	32.7	Roig and Boninsegna [1990]	-0.46	57.5	38.5	9	1.16	0.89
26	Balmaceda	Tree rings	1828	1988	71.75	45.9	ITRDB series arge023	0.31	75	48.5	4	1.11	0.8
27	Number of days with rain in Mendoza	Early Instrumental	1830	2006	68.78	32.8	Coni [1897]; Servicio Meteorologico Nacional de Argentina, pers. comm..	0.7	67	32.5	29		0.97
28	Cluster NWA 1	Tree rings	1833	2002	65	23	Villalba et al. [1992]	0.36	47.5	23.5	6	0.65	0.73
29	Paso de las Nubes 3	Tree rings	1848	1991	71.8	41.1	Villalba et al. [1997a]	-0.39	60.5	52	7	0.81	0.76
30	Rio de Janeiro	Instrumental	1851	1990	43.2	22.9	Peterson and Vose [1997; PV97]	0.96	43	23.5	23		1.12
31	Valdivia/Pichoy	Instrumental	1853	2000	73.1	39.8	PV97	0.96	73.5	40	27		0.95
32	Bahia Blanca	Instrumental	1860	2007	62.25	38.7	PV97	0.87	62.5	39	32		1.1
33	Buenos Aires	Instrumental	1861	2005	58.5	34.6	PV97	0.94	58.5	34.5	38		1.5
34	Concepción, Ñufo de chavez	Tree rings	1861	2005	62.13	16.4	unpublished (L. Lopez pers. comm. 2008)	0.48	63.5	23	12		0.95
35	Puerto Montt	Instrumental	1862	2007	73.1	41.4	PV97	0.9	73.5	41.5	33		1.01
36	Santiago Pudahuel	Instrumental	1867	2007	70.7	33.5	PV97	0.69	70	35	8		0.97
37	La Serena	Instrumental	1869	2007	71.2	29.9	PV97	0.44	71.5	34.5	4		0.9
38	Cordoba	Instrumental	1873	2002	64.2	31.3	PV97	0.88	64	32	36		0.94
39	Stanley	Instrumental	1874	1981	57.9	51.7	PV97	-0.46	64	22	16		0.74
40	Corrientes Aero	Instrumental	1875	2005	58.77	27.5	PV97	0.99	58.5	28	29		1.23
41	Rosario Aero	Instrumental	1875	2007	60.8	32.9	PV97	0.85	60	33	33		1.39
42	Salta Aero	Instrumental	1875	2006	65.48	24.9	PV97	0.75	65	24.5	10		0.85
43	Parana Aero	Instrumental	1876	2007	60.5	31.8	PV97	0.92	60.5	31	34		1.31
44	San Juan Aero	Instrumental	1876	2007	68.7	31.5	PV97	0.91	68	32	20		1.08
45	Santiago del Estero	Instrumental	1876	2006	64.3	27.8	PV97	0.96	64	27.5	32		1.07
46	Ushuaia Aero	Instrumental	1876	2004	68.3	54.8	PV97	0.97	65.5	55.5	28		1.11
47	Asuncion Aero	Instrumental	1877	2007	57.63	25.3	PV97	0.95	57.5	25.5	16		1.2
48	Rio Sala and Popayan	Tree rings	1881	2002	64.6	24.6	Villalba et al. [1992]	0.52	63.5	31	30		0.7
49	Curitiba	Instrumental	1885	2007	49.3	25.4	PV97	0.91	49.5	26	19		1.4
50	Quebrada de Humahuaca	Tree rings	1886	2001	65.33	23.2	Morales et al. [2004]	0.51	64.5	22.5	11		0.65

51	Sao Paulo	Instrumental	1887	2007	46.9	23.6	PV97	0.96	46	24	10	1.15
52	Mar del Plata Aero	Instrumental	1888	2007	57.6	37.9	PV97	0.92	57	37.5	27	0.94
53	Punta Arenas	Instrumental	1888	2007	70.9	53	PV97	0.95	71	54.5	19	1.23
54	Tornquist	Instrumental	1889	1995	62.22	38.1	PV97	0.87	61.5	38.5	35	1.04
55	Mendoza Obs.	Instrumental	1892	2001	68.9	32.9	PV97	0.89	68	32.5	33	0.87
56	O Higgins	Tree rings	1892	1999	72.5	48.5	Lara et al. [2005]	0.56	66	30.5	30	1.13
57	Esquel Aero	Instrumental	1896	2007	71.2	42.9	PV97	0.97	71	43	27	1.27
58	Villarrica	Instrumental	1898	2007	72.22	39.3	PV97	0.96	56.5	26	19	1.25
59	Guamini	Instrumental	1900	1992	62.4	37.1	PV97	0.88	62.5	37.5	45	1.14
60	Trelew Aero	Instrumental	1901	2007	65.3	43.2	PV97	0.71	66.5	44	18	1.59
61	Concordia Aero	Instrumental	1902	2007	58	31.3	PV97	0.97	58	31.5	30	1.02
62	Isla Robinson Crusoe	Instrumental	1902	2007	78.8	33.6	PV97	0.9	79	34.5	35	0.87
63	Santa Rosa	Instrumental	1902	2007	64.32	36.6	PV97	0.99	64	37	36	1.07
64	Catamarca Aero	Instrumental	1903	2007	65.8	28.5	PV97	0.93	65	29	21	1.14
65	La Quiaca Obs.	Instrumental	1903	2007	65.6	22.1	PV97	0.99	65.5	23	10	1.04
66	Posadas Aero	Instrumental	1903	2007	56	27.4	PV97	0.97	56.5	28	31	1.26
67	Victorica	Instrumental	1905	1995	65.43	36.2	PV97	0.98	65.5	37	32	0.96
68	Concepcion	Instrumental	1912	2007	73.1	36.8	PV97	0.94	73	37.5	34	1.03
69	Huinca Rananco	Instrumental	1912	1995	64.27	34.8	PV97	0.98	64.5	35	36	1.07
70	Punta Angeles	Instrumental	1912	1993	71.1	33	PV97	0.76	71.5	35	11	0.9
71	Temuco	Instrumental	1912	2007	72.8	38.8	PV97	0.9	72.5	39.5	40	1.04
72	Valdivia Town	Instrumental	1912	2007	73.1	40	PV97	1	73.5	40.5	28	0.96
73	Paso de los Libres	Instrumental	1918	2006	57.2	29.7	PV97	0.93	57.5	30	35	1.21
74	Rio Cuarto Aero	Instrumental	1918	2007	64.2	33.1	PV97	0.98	64	33.5	25	1.19

**Table S2:** Proxy records used for the austral winter (JJA) precipitation reconstructions. Start and end years are AD. The non-instrumental predictors are taken from the SSA proxy network of Neukom et al. [2010]. Columns nine to twelve quantify the Spearman correlations of the proxies with the instrumental grid 1931-1995: The highest absolute correlation (max. r; correlation at the “best location”), the coordinates of the “best location” and the percentage of grid cells with significant ( $p < 0.05$ ) correlations. The last four columns indicate the average relative regression weight of each predictor in the years 1590, 1700, 1850 and 1931, respectively (see also Figure S15).

Nr.	Name	Archive	Start	End	Lon W	Lat S	Reference	Correlation with instr. Gridboxes				Proxy Weight			
								max. r	Lon W	Lat S	% $p < 0.05$	1498	1700	1850	1931
1	106KL off Peruvian coast	Marine Sediment	-19402	1972	77.67	12.1	Rein [2007]	-0.39	65.5	31.5	5	0.99	0.91	0.89	1.04
2	Cluster CAN 20	Tree rings	182	1995	71.83	41.3	Villalba [1990b]; Lara et al. [2000]	-0.48	60	22.5	6	0.78	0.78	0.82	0.84
3	Cluster CAN 25	Tree rings	424	1990	71.83	42.5	Lara et al. [2000]	-0.47	65	32	12	1.01	0.65	1	0.89
4	El Asiento	Tree rings	1280	1972	70.82	32.5	La Marche et al. [1979b]	0.57	69.5	34.5	13	1.03	0.81	0.77	0.77
5	Caramavida	Tree rings	1548	1972	73.17	37.7	La Marche et al. [1979b]	-0.44	69	34.5	8	0.79	0.64	0.59	0.7
6	Cluster CAN 15	Tree rings	1566	1991	71.92	41.2	Villalba et al. [1997a]	0.37	62.5	40	9	1.53	1.37	1.54	1.06
7	Cluster CAN 26	Tree rings	1585	1987	73.83	42.5	Villalba [1990a]; Roig [1991]	-0.43	71.5	48	19	0.72	1.03	0.72	0.91
8	Santa Fe and Corrientes precipitation index	Documentary	1590	1805	60	30	Prieto [2007]; Neukom et al. [2009]	-0.32	64.5	55.5	2	1.15	1.18	1.09	1.21
9	Mendoza River runoff index	Documentary	1601	1960	68	32	Prieto et al. [1999a]; Neukom et al. [2009]	0.45	69	35.5	8	1.13	1.46	0.89	
10	Great Barrier Reef coral luminescence	Corals	1631	2005	-147	20	Lough [2007]	0.41	63.5	23.5	12	1.52	1.49	1.09	
11	Cluster CAN 3	Tree rings	1640	1975	71.25	38	La Marche et al. [1979a; 1979b]	-0.44	71.5	47	10	0.96	0.79	0.84	
12	F-T IDPO index	Corals	1650	2004	180	0.02	Linsley et al. [2008]	0.56	53	33.5	8	1.23	0.92	0.86	
13	New Caledonia $d^{18}O$	Corals	1657	1992	-166.5	22.5	Quinn et al. [1998]	0.44	68.5	29	11	0.81	0.77	1.15	
14	Volcan Lonquimay	Tree rings	1702	1975	71.57	38.4	La Marche et al. [1979b]	-0.49	68.5	34.5	14	0.75	0.68		
15	Secas $d^{18}O$	Corals	1707	1984	82.05	-7	Linsley et al. [1994]	0.51	68	33	28	1.52	0.89		
16	Cluster SAN 5	Tree rings	1725	1984	67.67	54.8	Boninsegna et al. [1989]	-0.42	65.5	32	7	1.12	1.03		
17	Cluster SAN 6	Tree rings	1731	1986	64.33	54.8	Boninsegna et al. [1989]	0.38	71.5	41.5	4	0.76	0.78		
18	Valle Ameghino	Tree rings	1743	1997	72.17	50.4	Masiokas and Villalba [2004]	0.38	46.5	24	8	0.68	1.1		
19	Santiago del Estero precipitation index	Documentary	1750	1921	64.27	27.8	Herrera et al. [2003]; Neukom et al. [2009]	0.45	61	25.5	13	1.44	1.36		
20	Great Barrier Reef Ba/Ca	Corals	1758	1998	-146	18	McCulloch et al. [2003]	-0.39	53.5	34	2	0.75	0.97		
21	Central Andes snow depth	Documentary	1760	1996	70	33	Prieto et al. [1999b]; Neukom et al. [2009]	0.45	68.5	34.5	17	0.93	0.8		
22	Paso Cordova	Tree rings	1760	1986	71.25	40.7	ITRDB series arge050	0.41	74	39	11	1.09	0.73		

23	Dyer Plateau 1	Ice Cores	1761	1970	65.45	71.1	Fisher [2002]	0.42	47	23	10	0.99	0.72
24	Dronning Maud Land	Ice Cores	1800	1999	0	75	Graf et al. [2002]	0.57	71	48	17	1.3	1.32
25	Rio Foyel	Tree rings	1803	1982	71.42	41.7	Roig [1991]	-0.48	68.5	34.5	23	1.03	1.03
26	Cisnes	Tree rings	1811	1997	71.7	44.7	Lara et al. [2005]	-0.37	51	29.5	5	1.01	0.84
27	Chapelco	Tree rings	1822	1985	71.23	40.3	ITRDB series arge029	-0.38	62	38.5	4	0.77	0.91
28	Avaiki	Speleothems	1829	2001	169.8	19	Rasbury and Aharon [2006]	-0.4	65	32.5	10	0.99	0.79
29	Number of days with rain in Mendoza	Early Instrumental	1830	2006	68.78	32.8	Coni [1897]; Servicio Meteorologico Nacional de Argentina, pers. comm.	0.8	68.5	33	39		0.95
30	Rio de Janeiro	Instrumental	1851	1990	43.2	22.9	Peterson and Vose [1997; PV97]	0.94	43	23.5	17		0.97
31	Valdivia/Pichoy	Instrumental	1853	2000	73.1	39.8	PV97	0.91	73.5	40.5	19		0.81
32	Cluster NWA 4	Tree rings	1858	1999	65	24	Villalba et al. [1992]	0.38	72.5	45.5	7		1.21
33	Bahia Blanca	Instrumental	1860	2007	62.25	38.7	PV97	0.91	62.5	39	25		1.32
34	Buenos Aires	Instrumental	1861	2005	58.5	34.6	PV97	0.94	58.5	35	38		1.19
35	Puerto Montt	Instrumental	1862	2007	73.1	41.4	PV97	0.88	74	41.5	16		1.08
36	Santiago Pudahuel	Instrumental	1867	2007	70.7	33.5	PV97	0.92	70.5	34	23		1.34
37	La Serena	Instrumental	1869	2007	71.2	29.9	PV97	0.99	71.5	30	42		1.05
38	Cordoba	Instrumental	1873	2002	64.2	31.3	PV97	0.96	64	32	32		1.28
39	Stanley	Instrumental	1874	1981	57.9	51.7	PV97	0.48	74	40.5	14		0.92
40	Corrientes Aero	Instrumental	1875	2005	58.77	27.5	PV97	0.89	58.5	27.5	42		0.93
41	Rosario Aero	Instrumental	1875	2007	60.8	32.9	PV97	0.92	60	32.5	39		1.01
42	Salta Aero	Instrumental	1875	2006	65.48	24.9	PV97	0.76	65.5	24	23		0.94
43	Parana Aero	Instrumental	1876	2007	60.5	31.8	PV97	0.94	60.5	31.5	28		1.02
44	San Juan Aero	Instrumental	1876	2007	68.7	31.5	PV97	0.82	69	31.5	16		1.03
45	Santiago del Estero	Instrumental	1876	2006	64.3	27.8	PV97	0.95	64	27.5	34		0.87
46	Ushuaia Aero	Instrumental	1876	2004	68.3	54.8	PV97	0.72	68.5	56	18		1
47	Asuncion Aero	Instrumental	1877	2007	57.63	25.3	PV97	0.96	57	25.5	34		1.09
48	Curitiba	Instrumental	1885	2007	49.3	25.4	PV97	0.98	49.5	26	19		1.1
49	Dique Escaba	Tree rings	1887	1985	65.78	27.7	Villalba et al. [1992]	0.4	65	31	10		1.07
50	Sao Paulo	Instrumental	1887	2007	46.9	23.6	PV97	0.96	46	24	21		0.81
51	Mar del Plata Aero	Instrumental	1888	2007	57.6	37.9	PV97	0.99	57	38	17		0.85
52	Punta Arenas	Instrumental	1888	2007	70.9	53	PV97	1	70.5	54	15		1
53	Tornquist	Instrumental	1889	1995	62.22	38.1	PV97	0.87	62.5	38.5	47		1.19

54	Mendoza Obs.	Instrumental	1892	2001	68.9	32.9	PV97	0.87	68.5	33	43	0.91
55	Esquel Aero	Instrumental	1896	2007	71.2	42.9	PV97	0.98	71.5	42.5	27	0.81
56	Villarrica	Instrumental	1898	2007	72.22	39.3	PV97	0.97	56.5	26	43	1.25
57	Guamini	Instrumental	1900	1992	62.4	37.1	PV97	0.9	62	38	24	0.97
58	Neuquen Aero	Instrumental	1900	2006	68	39	PV97	0.88	69.5	40.5	25	1.12
59	Trelew Aero	Instrumental	1901	2007	65.3	43.2	PV97	0.98	65.5	44	30	1.38
60	Concordia Aero	Instrumental	1902	2007	58	31.3	PV97	0.95	58	32	19	1.46
61	Isla Robinson Crusoe	Instrumental	1902	2007	78.8	33.6	PV97	0.91	79	34.5	14	0.81
62	Santa Rosa	Instrumental	1902	2007	64.32	36.6	PV97	0.93	64.5	36.5	36	1
63	Catamarca Aero	Instrumental	1903	2007	65.8	28.5	PV97	0.88	65	29	22	0.86
64	La Quiaca Obs.	Instrumental	1903	2007	65.6	22.1	PV97	0.83	65	23	13	0.78
65	Posadas Aero	Instrumental	1903	2007	56	27.4	PV97	0.98	56	28	49	1.03
66	Victorica	Instrumental	1905	1995	65.43	36.2	PV97	0.93	65.5	36.5	33	0.87
67	Concepcion	Instrumental	1912	2007	73.1	36.8	PV97	0.9	72	37	25	1.13
68	Huinca Rananco	Instrumental	1912	1995	64.27	34.8	PV97	0.94	64.5	35	43	0.7
69	Punta Angeles	Instrumental	1912	1993	71.1	33	PV97	0.94	71.5	34	31	0.84
70	Temuco	Instrumental	1912	2007	72.8	38.8	PV97	0.87	72	38.5	19	1.35
71	Valdivia Town	Instrumental	1912	2007	73.1	40	PV97	0.99	73.5	40.5	25	1.37
72	Paso de los Libres	Instrumental	1918	2006	57.2	29.7	PV97	0.95	57	29.5	30	1.24
73	Rio Cuarto Aero	Instrumental	1918	2007	64.2	33.1	PV97	0.97	64	33.5	24	0.87

## References

- Argollo, J., et al. (2004), Potencialidad dendrocronológica de *Polylepis tarapacana* en los Andes Centrales de Bolivia, *Ecol. Boliv.*, 39, 5-24.
- Boninsegna, J. A., et al. (1989), Dendrochronological studies in Tierra del Fuego, Argentina, *Quaternary South Am.*, 7, 315-326.
- Briffa, K. R., et al. (1986), Climate Reconstruction from Tree Rings: Part 2, spatial Reconstruction of Summer Mean Sea-Level Pressure Patterns over Great Britain, *J. Climatol.*, 6, 1-15.
- Coni, E. R. (1897), *Saneamiento de la provincia de Mendoza*, Imprenta de Pablo E. Coni é Hijos, Buenos Aires.
- Cook, E. R., et al. (1994), Spatial Regression Methods in Dendroclimatology - a Review and Comparison of 2 Techniques, *Int. J. Climatol.*, 14, 379-402.
- Cook, E. R., et al. (2000), Warm-season temperatures since 1600 BC reconstructed from Tasmanian tree rings and their relationship to large-scale sea surface temperature anomalies, *Clim. Dynam.*, 16, 79-91.
- Fisher, D. A. (2002), High-resolution multiproxy climatic records from ice cores, tree-rings, corals and documentary sources using eigenvector techniques and maps: assessment of recovered signal and errors, *Holocene*, 12, 401-419.
- Garreaud, R. D., et al. (2009), Present-day South American climate, *Palaeogeogr. Palaeoclimatol.*, 281, 180-195.
- Gioda, A., and M. R. Prieto (1999a), Histoire des sécheresses andines. Potosí, El Niño et le Petit Age Glaciaire, *Revue de la Société Météorologique de France. La Météorologie*, 27, 33-42.
- Gioda, A., and M. R. Prieto (1999b), Para una historia climática de La Paz en los últimos cinco siglos. Historias de la ciudad de La Paz, Bolivia, *Revista de la coordinadora de Historia*, 3, 13-33.
- Graf, W., et al. (2002), Stable-isotope records from Dronning Maud Land, Antarctica, *Ann. Glaciol.*, 35, 195-201.
- Herrera, R., et al. (2003), Floods in the semiarid Argentinean Chaco during the 17th to 19th centuries, in *Proceedings of Palaeofloods, Historical Data & Climatic Variability: Applications in Flood Risk Assessment*, edited by V. R. Thorndyraft, et al., pp. 107-112, CSIC-Centro de Ciencias Medioambientales, Madrid.
- Kuhnert, H., et al. (1999), A 200-year coral stable oxygen isotope record from a high-latitude reef off western Australia, *Coral Reefs*, 18, 1-12.
- Lamarche, V. C., et al. (1979a), *Tree-ring chronologies of the southern hemisphere: Vol. 1: Argentina. Chronology Series V*, Laboratory of Tree-Ring Research, University of Arizona, Tucson, AZ.
- Lamarche, V. C., et al. (1979b), *Tree-ring chronologies of the southern hemisphere: Vol. 2: Chile. Chronology Series V*, Laboratory of Tree-Ring Research, University of Arizona, Tucson, AZ.
- Lara, A., et al. (2001), Dendroclimatology of high-elevation *Nothofagus pumilio* forests at their northern distribution limit in the central Andes of Chile, *Can. J. Forest. Res.*, 31, 925-936.
- Lara, A., and R. Villalba (1993), A 3620-Year Temperature Record from Fitzroya-Cupressoides Tree Rings in Southern South-America, *Science*, 260, 1104-1106.
- Lara, A., et al. (2000), Desarrollo de una red de cronologías de Fitzroya Cupressoides (Alerce) para Chile y Argentina, in *Dendrochronología en América Latina*, edited by F. Roig, pp. 193-215, Editorial Nacional de Cuyo, Mendoza.
- Lara, A., et al. (2008), A 400-year tree-ring record of the Puelo River summer-fall streamflow in the Valdivian Rainforest eco-region, Chile, *Clim. Change*, 86, 331-356.

Lara, A., et al. (2005), Spatial and temporal variation in *Nothofagus pumilio* growth at tree line along its latitudinal range (35 degrees 40 '-55 degrees S) in the Chilean Andes, *J. Biogeogr.*, *32*, 879-893.

Le Quesne, C., et al. (2009), Long-term glacier variations in the Central Andes of Argentina and Chile, inferred from historical records and tree-ring reconstructed precipitation, *Palaeogeogr. Palaeoclimatol.*, *281*, 334-344.

Linsley, B. K., et al. (1994), A Coral-Based Reconstruction of Intertropical Convergence Zone Variability over Central-America since 1707, *J. Geophys. Res.-Oceans*, *99*, 9977-9994.

Linsley, B. K., et al. (2008), Interdecadal-decadal climate variability from multicoral oxygen isotope records in the South Pacific Convergence Zone region since 1650 A.D, *Paleoceanography*, *23*, PA2219.

Lough, J. M. (2007), Tropical river flow and rainfall reconstructions from coral luminescence: Great Barrier Reef, Australia, *Paleoceanography*, *22*, PA2218.

Masiokas, M., and R. Villalba (2004), Climatic significance of intra-annual bands in the wood of *Nothofagus pumilio* in southern Patagonia, *Trees-Struct. Funct.*, *18*, 696-704.

McCulloch, M., et al. (2003), Coral record of increased sediment flux to the inner Great Barrier Reef since European settlement, *Nature*, *421*, 727-730.

Mitchell, T. D., and P. D. Jones (2005), An improved method of constructing a database of monthly climate observations and associated high-resolution grids, *Int. J. Climatol.*, *25*, 693-712.

Morales, M. S., et al. (2004), Rainfall-controlled tree growth in high-elevation subtropical treelines, *Ecology*, *85*, 3080-3089.

Neukom, R., et al. (2010), Multiproxy summer and winter surface air temperature field reconstructions for southern South America covering the past centuries, *Clim. Dynam.*, doi:10.1007/s00382-00010-00793-00383.

Neukom, R., et al. (2009), An extended network of documentary data from South America and its potential for quantitative precipitation reconstructions back to the 16th century, *Geophys. Res. Lett.*, *36*, L12703.

Peterson, T. C., and R. S. Vose (1997), An overview of the global historical climatology network temperature database, *Bull. Amer. Meteorol. Soc.*, *78*, 2837-2849.

Piovano, E. L., et al. (2009), Hydrological Variability in South America Below the Tropic of Capricorn (Pampas and Patagonia, Argentina) During the Last 13.0 Ka, in *Past Climate Variability in South America and Surrounding Regions*, edited by F. Vimeux, et al., pp. 323-351, Springer.

Prieto, M. R. (2007), ENSO signals in South America: rains and floods in the Parana River region during colonial times, *Clim. Change*, *83*, 39-54.

Prieto, M. R., and R. Herrera (2001), De sequías, hambrunas , plagas y “otras varias y continuas calamidades acaecidas en la Jurisdicción de Córdoba” durante el siglo XVIII, *Serie Economía y Sociedad. Cuadernos de Historia*, *4*, 131-158.

Prieto, M. R., et al. (1999a), Historical evidences of streamflow fluctuations in the Mendoza River, Argentina, and their relationship with ENSO, *Holocene*, *9*, 473-481.

Prieto, M. R., et al. (1999b), Snowfall and floods in the oriental slope of Argentinean-Chilean Andes from the Middle of the 18th century to the End the 19th century. Its relationship with ENSO. Extended Abstract. Conference on Reconstructing Climatic variability from Historical Sources and Other Proxy Records. Earth System History Program of the U. S NSF and the Office of Global Programs of the U.S NOAA, Manzanillo , México.

Prieto, M. R., et al. (2000), Archival evidence for some aspects of historical climate variability in Argentina and Bolivia during the 17th and 18th centuries., in *Southern Hemisphere Paleo and Neo-Climates: Methods and Concepts*, edited by P. P. Smolka and W. Volkheimer, pp. 127-142, Springer, Berlin.

- Quinn, T. M., et al. (1998), A multicentury stable isotope record from a New Caledonia coral: Interannual and decadal sea surface temperature variability in the southwest Pacific since 1657 AD, *Paleoceanography*, 13, 412-426.
- Rasbury, M., and P. Aharon (2006), ENSO-controlled rainfall variability records archived in tropical stalagmites from the mid-ocean island of Niue, South Pacific, *Geochem. Geophys. Geosyst.*, 7, Q07010.
- Rein, B. (2007), How do the 1982/83 and 1997/98 El Niños rank in a geological record from Peru?, *Quatern. Int.*, 161, 56-66.
- Roig, F. (1991), Dendrocronología y dendroclimatología del bosque de Pilgerodendron uviferum en su área norte de dispersión, *Bul. Soc. Argent. Bot.*, 27, 217-234.
- Roig, F., and J. Boninsegna (1990), Environmental factors affecting growth of Adesmia communities as determined from tree rings, *Dendrochronologia*, 8, 39-65.
- Schmelter, A. (2000), Climatic response and growth-trends of Nothofagus pumilio along altitudinal gradients from arid to humid sites in northern Patagonia - A progress report, in *Dendrochronología en América Latina*, edited by F. Roig, pp. 193-215, Editorial Nacional de Cuyo, Mendoza.
- Schneider, D. P., et al. (2006), Antarctic temperatures over the past two centuries from ice cores, *Geophys. Res. Lett.*, 33, L16707.
- Soliz, C., et al. (2009), Spatio-temporal variations in Polylepis tarapacana radial growth across the Bolivian Altiplano during the 20th century, *Palaeogeogr. Palaeoclimatol.*, 281, 296-308.
- Villalba, R. (1990a), Climatic Fluctuations in Northern Patagonia During the Last 1000 Years as Inferred from Tree-Ring Records, *Quaternary Research*, 34, 346-360.
- Villalba, R. (1990b), Latitude of the surface high-pressure belt over western South America during the last 500 years as inferred from tree-ring analysis, *Quaternary South Am.*, 7, 273-303.
- Villalba, R. (2007), Tree-ring evidence for tropical-extratropical influences on climate variability along the Andes in South America, *PAGES News*, 15, 23-25.
- Villalba, R., et al. (1997a), Recent trends in tree-ring records from high elevation sites in the Andes of northern Patagonia, *Clim. Change*, 36, 425-454.
- Villalba, R., et al. (1997b), Sea-level pressure variability around Antarctica since AD 1750 inferred from subantarctic tree-ring records, *Clim. Dynam.*, 13, 375-390.
- Villalba, R., et al. (1998), Tree-ring based reconstructions of northern Patagonia precipitation since AD 1600, *Holocene*, 8, 659-674.
- Villalba, R., et al. (1992), Spatial Patterns of Climate and Tree Growth Variations in Subtropical Northwestern Argentina, *J. Biogeogr.*, 19, 631-649.
- Villalba, R., and T. T. Veblen (1997), Regional patterns of tree population age structures in northern Patagonia: Climatic and disturbance influences, *J. Ecol.*, 85, 113-124.